

# Perspective on defect characterization in semiconductors by positron annihilation spectroscopy

Cite as: J. Appl. Phys. 135, 040901 (2024); doi: 10.1063/5.0180024

Submitted: 6 October 2023 · Accepted: 30 December 2023 ·

Published Online: 23 January 2024



View Online



Export Citation



CrossMark

Ilja Makkonen<sup>1,a)</sup>  and Filip Tuomisto<sup>2,b)</sup> 

## AFFILIATIONS

<sup>1</sup> Department of Physics, University of Helsinki, P.O. Box 43, FI-00014 University of Helsinki, Helsinki, Finland

<sup>2</sup> Department of Physics and Helsinki Institute of Physics, University of Helsinki, P.O. Box 43, FI-00014 University of Helsinki, Helsinki, Finland

**Note:** This paper is part of the Special Topic on Native Defects, Impurities and the Electronic Structure of Compound Semiconductors: A Tribute to Dr. Wladyslaw Walukiewicz.

**a) Author to whom correspondence should be addressed:** [ilja.makkonen@helsinki.fi](mailto:ilja.makkonen@helsinki.fi)

**b) Electronic mail:** [filip.tuomisto@helsinki.fi](mailto:filiptuomisto@helsinki.fi)

## ABSTRACT

This Perspective focuses on experimental and theoretical aspects of positron annihilation spectroscopy. This set of methods is highly suitable for identifying and quantifying vacancy-type defects in semiconductors and also allows for analyzing their physics characteristics. We present selected examples from the past decade, where the methods have been used for obtaining timely and useful insights into the defect-controlled phenomenon in narrow-gap (Ge, GaSb) and wide-gap (III-nitride, oxide) semiconductors. We also discuss possible future developments that may allow more detailed studies in novel semiconductor materials and devices with ever more complex lattice structures.

27 January 2024 13:37:47

Published under an exclusive license by AIP Publishing. <https://doi.org/10.1063/5.0180024>

## I. INTRODUCTION

Point defects in semiconductors are the fundamental reason behind the usefulness of this class of materials. The type of electrical conduction of a semiconductor is controlled by adding dilute—as low as ppb level—amounts of impurity atoms to the semiconductor lattice. However, at the same time, it is very hard, if not impossible, to avoid similar or higher levels of unwanted impurities. In addition, nature has it so that point defects intrinsic to the host lattice are relatively easily formed during manufacturing of the materials and devices. Of these intrinsic point defects, vacancies (vacant lattice sites, that is, missing atoms) tend to be the most energetically favorable.<sup>1</sup> They may cause electrical compensation either through direct passivation of the impurity dopants or by providing carrier traps in the semiconductor bandgap. They may also act as non-radiative recombination centers, produce parasitic luminescence, and cause optical absorption, all detrimental to the required properties of semiconductors employed in opto-electronic devices.

Direct experimental characterization of vacancy defects is hard. Simultaneous determination of their identity (atomic structure), quantity (density, distribution), as well as electrical, optical, and mechanical characteristics is very rarely possible. Most experimental methods for defect characterization focus on one of the various aspects: atomic structure, electrical levels in the bandgap, or optical characteristics. Vacancy defects are particularly challenging as many of the structure-sensitive methods cannot detect empty space.

Positrons provide a selective sensitive probe for vacancy-type defects in semiconductors.<sup>2</sup> The electrostatic repulsion of the positive ion cores in a crystalline solid drives a positron into a delocalized state in the interstitial space of the lattice. At the site of vacancy, there is a lack of positive charge, creating a potential well for the positron. The positron–electron annihilation behavior changes measurably when a positron is trapped at such a vacancy site, allowing for the identification and quantification of vacancy defects. The trapping and annihilation process of positrons does not depend on the conductivity or the bandgap of the semiconductor. Hence, from the point of

view of the experiment, there is no difference between narrow gap semiconductors, ultra-wide gap semiconductors, metals, and insulators. Optical properties do not affect the experiments either.

In this Perspective, we provide a brief introduction to the experimental and theoretical-computational aspects of positron annihilation spectroscopy. In-depth reviews of the methods are found elsewhere (see, for example, Refs. 2–4 and the references therein). We review a few recent examples of experimental results in narrow-gap and (ultra-)wide-gap semiconductor materials, as well as recent developments in theoretical developments that give a significant boost to the identification of defects. Finally, we present our expectations of new developments in positron annihilation spectroscopy applied in semiconductor physics and technology.

## II. POSITRON ANNIHILATION: EXPERIMENT AND THEORY

In positron annihilation experiments for defect characterization in solids, one positron at a time is injected into a sample to ensure

the sensitivity to the lattice structure, avoiding positron–positron interactions. This also allows for quite straightforward theoretical treatment of the situation. When an energetic positron enters a crystal, it rapidly loses its kinetic energy and thermalizes, finishing in a delocalized Bloch-like state in the lattice as illustrated in Fig. 1(a). This process take a few picoseconds, a time that is short compared to the ensuing trapping and annihilation processes. The positron will annihilate with an electron in the lattice, either when in the delocalized state or as trapped at a defect—see Fig. 1(b) that illustrates the density of positron trapped at a vacancy. The annihilation rate of the positron, the inverse of the positron lifetime, is directly proportional to the overlap of the positron and electron densities in the lattice. The annihilation rate slows down and the positron lifetime becomes longer if the positron density is localized at the vacancy, as the electron density is locally reduced at a vacancy. Also, the energy distribution of the annihilation photons—roughly, 511 keV each, in the two-photon positron–electron annihilation process—changes for a trapped positron due to the difference in the electron momentum

27 January 2024 13:37:47

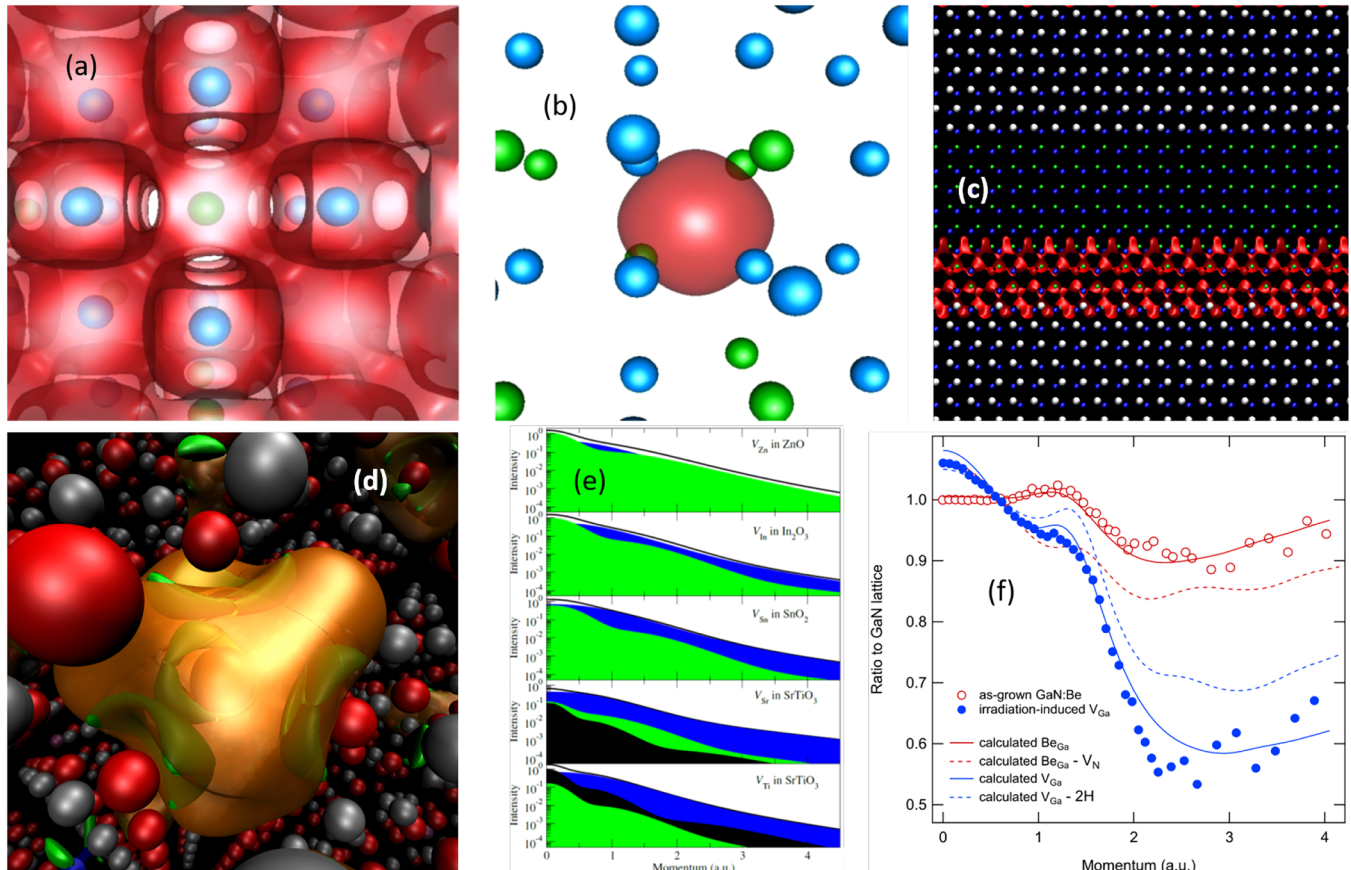


**FIG. 1.** Schematic representations of (a) a free positron's density isosurface (red delocalized isosurface) in a binary crystal lattice represented by blue and green spheres, (b) localized positron at a monovacancy defect in the same crystal, (c) positron (red density isosurface) confined at an interface in a polar GaN/AlN heterostructure (see Ref. 5), and (d) trapped at a substitutional Be on the Ga site in GaN (orange density isosurface, see Ref. 6). Panel (e) presents an approximate decomposition of computational Doppler broadening spectra of positrons annihilating at vacancies in metal oxides to oxygen (blue), cation A (green) and cation B (black) contributions (see Ref. 7). Panel (f) shows experimental and calculated Doppler broadening ratio curves for a substitutional Be on the Ga site and a Ga vacancy, with associated complexes (see Ref. 6).

density of the annihilating electrons. In the most simple view, the Doppler broadening of the 511 keV annihilation line narrows due to a reduced annihilation rate with electrons on atomic core levels that have a wide momentum distribution. The same phenomenon also changes the angular distribution of the annihilation photons, but this property is rarely utilized in defect studies. In practice, the concentration sensitivity range for vacancy defects is roughly from  $10^{15}$  to  $10^{19} \text{ cm}^{-3}$ .

Even if the conductivity of the material is not a limiting factor for positron annihilation experiments, the lack of efficient screening of Coulomb attraction and repulsion in semiconductors is beneficial for defect studies. Vacancy defects in a negative charge state exhibit a temperature dependence in their trapping efficiency for positrons, thanks to the amplification of the positron wave function at the center of the vacancy.<sup>8</sup> This makes negatively charged vacancy defects more efficient positron traps than neutral vacancy defects, while positively charged vacancies effectively repel positrons. The trapping coefficient (equivalent to a capture cross section for charge carriers) for negatively charged vacancies is proportional to  $T^{-1/2}$ , and at room temperature, roughly twice that of neutral vacancy defects. Performing experiments as a function of sample temperature hence provides the means to distinguish between negative and neutral charge states of vacancy defects. Defect charge states can be manipulated by, e.g., illumination of the samples during experiments, allowing for characterization of optical transition levels of the vacancy defects.

Positrons can also get trapped at Rydberg states of negatively charged defects even if they do not have any open volume, such as acceptor impurities. However, the low binding energy (typically, 30–70 meV) of these shallow states leads to efficient escape of the trapped positrons at elevated temperatures. Hence, the negative ion like defects are efficient positron traps usually below room temperature. As the Bohr radius of such a state is large compared to the inter-atomic distance in the lattice, a positron trapped at a negative ion will exhibit identical annihilation characteristics with the delocalized state in the lattice. This means that the negative ions can only be detected when they compete in positron trapping with vacancy defects at low temperatures.

## A. Experimental aspects

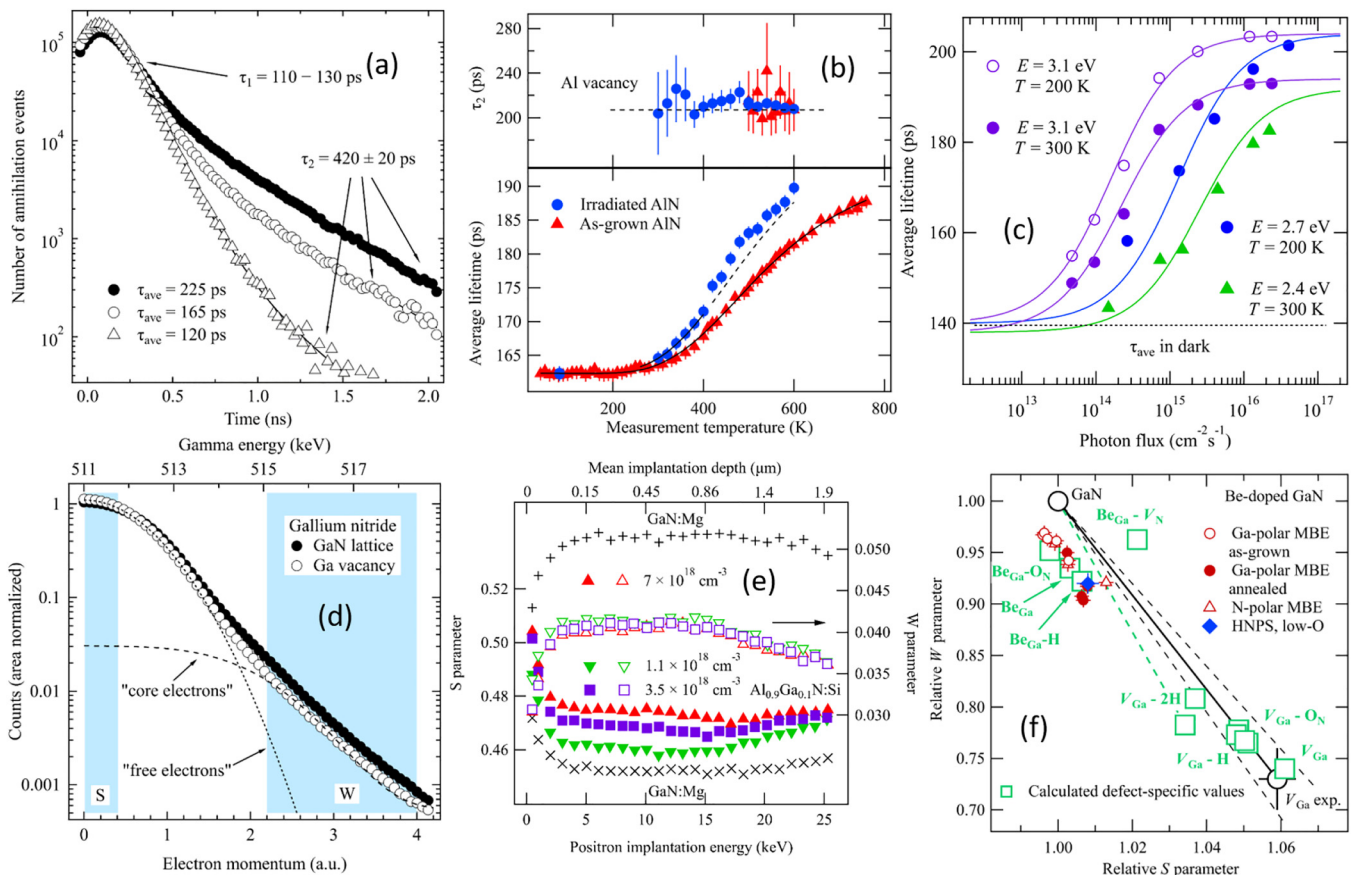
The most simple experimental approach to positron annihilation spectroscopy is to sandwich a  $\beta^+$  active (positron emitting) isotope between two identical sample pieces, ensuring that all emitted positrons enter the samples.  $^{22}\text{Na}$  has the advantage of the emission of a 1.27 MeV photon nearly simultaneously with the positron, providing a start signal for measuring positron lifetimes. The measured positron lifetime spectrum is a sum of exponential decay components  $\lambda_i$ , each representing positron annihilations in different states  $i$ : either as trapped at a vacancy defect or “free” annihilations in the lattice  $n(t) = \sum_i I_i \exp(-\lambda_i t)$ , where the sum of the intensities  $I_i$  is  $\sum_i I_i = 1$ . Figure 2(a) shows a few examples of positron lifetime spectra measured in natural diamond with relatively large vacancy clusters.<sup>9</sup> The intensities of the lifetime components carry information of the concentration of each vacancy defect, while the magnitudes of the decay constants ( $\lambda_i = \tau_i^{-1}$ ) correspond to the size of each vacancy defect. An important and

statistically very accurate parameter is the average positron lifetime  $\tau_{\text{ave}} = \sum_i I_i \tau_i$  that coincides with the center-of-mass of the lifetime spectrum. When positrons annihilate as trapped at vacancies  $\tau_{\text{ave}}$  increases above the positron lifetime in the lattice  $\tau_B$ , called the bulk lifetime.

Measurements as a function sample temperature reveal important information about the charge states of the detected defects. Figure 2(b) shows  $\tau_{\text{ave}}$  measured as a function of temperature in as-grown and irradiated AlN crystals.<sup>10</sup> The lifetime spectra at elevated temperatures exhibited two components in these samples, with the second (longer) component corresponding to Al vacancies with a lifetime  $\tau_2 = 210 \pm 5 \text{ ps}$ . The temperature dependence of  $\tau_{\text{ave}}$  is typical of the situation where negative ion like defects compete with vacancies in positron trapping at (relatively) low temperatures. The behavior can be analyzed in detail and a temperature-dependent trapping model fitted to the experimental data, revealing that the Al vacancies are in the negative charge state, and both the concentrations of the Al vacancies and of negative ions can be determined. Figure 2(c) shows another example where natural diamond is illuminated with different wavelength and varying intensity during positron annihilation experiments.<sup>11</sup> The illumination changes the charge state of the vacancy clusters and detailed analysis can be performed assuming a simple model of electron excitation and recombination.

The Doppler broadening of the 511 keV annihilation line is often analyzed by determining parameters describing the shape of the line:  $S$  is the fraction of annihilation events in the central part of the peak, originating from annihilations with low momentum electrons, while  $W$  is the fraction of annihilations with high momentum electrons, as shown in Fig. 2(d). Typical momentum ranges are 0–0.4 a.u. for the  $S$  parameter and above 2.0 a.u. for the  $W$  parameter. While these parameters have no direct physical interpretation, most of the low momentum annihilation events are with electrons that are not bound to atomic core levels, i.e., “free,” and exhibit a relatively narrow Gaussian (free particle-like) momentum distribution. Similarly, core electrons that have a wider momentum distribution dominate the annihilations in the high momentum range. Doppler broadening experiments are performed in the above-described sandwich configuration and also employing variable-energy positron beams. Such beams, where the kinetic energy of the positrons is typically tuned in the range 0–50 keV, allow studying near-surface regions, thin films, and multi-layer structures. Figure 2(e) shows the  $S$  and  $W$  parameters measured as a function of positron implantation energy in selected  $\text{Al}_{0.9}\text{Ga}_{0.1}\text{N}$  thin films doped with Si.<sup>12</sup> At low implantation energies, the implanted positrons can diffuse back to the surface and annihilate in surface states. In Fig. 2(e), the data obtained at positron energies in the range 5–15 keV correspond to positrons annihilating inside the thin film, and at higher energies, positrons also detect the substrate material. Also, positron lifetime can be measured with a variable-energy positron beam but requires more complicated systems for generating the required timing information.<sup>13</sup>

Vacancy defects have different “fingerprints” in the so-called S-W plot shown in Fig. 2(f). In this plot, the  $S$  and  $W$  parameters are normalized with those of a defect-free reference sample of the material under study. Each defect has a different pair of  $S$  and  $W$  parameters, shown by the large square symbols in Fig. 2(f)—note



27 January 2024 13:37:47

**FIG. 2.** (a) Experimental positron lifetime spectra with two components, measured in natural diamond samples containing large vacancy clusters (see Ref. 9). (b) Average positron lifetime and the second lifetime component extracted from the lifetime spectra in as-grown and irradiated AlN crystals (see Ref. 10). (c) Average positron lifetime as a function of illumination flux and photon energy in natural diamond with large vacancy clusters (see Ref. 11). (d) Folded experimental coincidence Doppler broadening spectra for the GaN lattice and Ga vacancy. Typical integration windows for  $S$  and  $W$  parameters are shown (see Ref. 2). (e)  $S$  and  $W$  parameters as a function of positron implantation energy and corresponding mean implantation depth in selected MOVPE Si-doped AlGaN alloys measured at room temperature. The data for a Mg-doped GaN reference is also shown (see Ref. 12). (f) Relative ( $S$ ,  $W$ ) parameters measured in Be-doped GaN. Theoretically calculated parameters for a variety of defects are shown in addition to the experimentally determined ( $S$ ,  $W$ ) parameters typical of isolated Ga vacancies in GaN (see Ref. 6).

that the green symbols are obtained from theoretical calculations discussed below. If a GaN sample contains, e.g.,  $V_{\text{Ga}}-\text{O}_N$  complexes as the dominant vacancy defect species, the data point measured in the sample will be on the line connecting the GaN and  $V_{\text{Ga}}-\text{O}_N$  points in the plot, and the position on the line determines the concentration of these defects. Figure 2(f) shows experimental data from Be-doped GaN thin films where the annihilations take place predominantly in  $\text{Be}_{\text{Ga}}$  defects that are fundamentally a Ga vacancy decorated by a small Be atom.<sup>6</sup>

## B. Theory/computation aspects

The measured positron annihilation parameters, such as positron lifetime components and the Doppler line shape, provide only indirect information on the defects in the sample. Experiments benefit strongly from supportive modeling of defects, their electronic

structure, and the positrons annihilating at them.<sup>2</sup> These quantities can be modeled for a given candidate defect model and compared directly with experiment. Currently, the theory development is aiming at enabling various many-body quantum methods to be used in connection with topical experiments (see Sec. IV C). The most practical and widely used method has been the two-component electron–positron density functional theory,<sup>14</sup> whose practical application involves parametrized approximations for the electron–positron correlation energy and the so-called enhancement factor, which takes into account the many-body screening of the positron by electrons and how this affects, e.g., the positron annihilation rate. Modeling the Doppler broadening related to the momentum density of annihilating pairs is not an exact quantity even in the exact two-component density-functional theory and requires further approximations.

The starting point in the practical modeling of behavior and annihilation positrons in solids in connection with experiments is

often a density-functional calculation with a state-of the art electronic-structure code. Typically, plane waves, periodic boundary conditions, and either pseudopotentials or the projector-augmented wave method are applied. Defects are modeled using supercell models with tens or hundreds of atoms. Since in a typical experimental scenario, there is only one positron in the sample at a time, one positron is added into the ion-electron system. As the phenomena of positron thermalization and trapping are a couple of orders of magnitude faster than positron annihilation, it is perfectly sufficient to consider the electronic and positronic ground state. The calculation tells whether the positron prefers a free delocalized state [Fig. 1(a)] in scope of the model and approximations used or to lower the Coulomb repulsion of nuclei by trapping at the defect instead [Fig. 1(b)]. We can also look at nanostructures such as III-nitride heterostructures and use modeling to understand the sensitivity of the positrons to different regions of the samples [Fig. 1(c)]. The two-component functionals and momentum density models provide estimates for the positron lifetime  $\tau_i$  and Doppler line shape associated with the positron trap modeled. These results can then be compared directly with experiments. At best, the comparison can lead to a precise identification of the open-volume defects behind the signal in positron measurements or at least provide a microscopic explanation to observed trends. The positron lifetime component  $\tau_i$  corresponding to a given defect mostly provides information on the size of the open volume at the vacancy or vacancy cluster but is insensitive to the chemical surroundings. On the other hand, the fine details of the Doppler-broadened 511 keV annihilation line, which reflects the electron momentum density at the annihilation site, can contain much information on the identity of the atoms surrounding the site. The examples in Sec. III highlight the recent achievements in the field, in which modeling has played a key role.

The shape of the 511 keV annihilation line [Fig. 2(d)] reflects primarily the size of the open volume at the vacancy (narrowing effect with increasing size due to reduced contact with high-momentum core electrons—most often there is a correlation between  $S$  and  $\tau_i$ ) but even more importantly also chemical “fingerprints” of core shells of elements in the first (and sometimes also second) coordination shell of the vacancy defect. Ideally, a measurement for a defect-free reference sample is needed so that trends seen in experiment and theory can be compared with equal footing. The best measurement for real defect identification is based on measuring the full line shape using a slow positron beam (no source contribution) and a  $2\gamma$  coincidence measurement requiring energy conservation (good peak-to-background ratio enabling access to the high-momentum region dominated by core electrons). It is often customary to compare experiment with theory using a so-called “ratio plot”, in which the experimental spectrum is represented as a ratio to the reference spectrum and the computational one is divided by the computational result for the defect-free lattice. This enables some error cancelation (mainly on the theory side) and an easier comparison at all momentum regions and intensity scales. For instance, if we take the data in Fig. 2(d) and divide the “Ga-vacancy” spectrum by the “GaN lattice spectrum,” we obtain the ratio curve shown in Fig. 1(f). The shape of the  $V_{\text{Ga}}$  ratio curve arises from the increased contact (in a relative sense) with low-momentum electrons at the vacancy and

decreased contact with high-momentum bound electrons of N and Ga (mainly, Ga 3d). The Ga vacancy can be clearly distinguished from the  $\text{Be}_{\text{Ga}}$  antisite, which also happens to trap positrons [see Fig. 1(d), Ref. 6 and the discussion below].

Figure 1(e) exemplifies the “fingerprints” different elements can display in positron studies of metal oxides.<sup>7</sup> Various trends seen in measurements could be explained by a differing average number of O ions around annihilation sites (or conversely, the average number oxygen vacancies complexed with cation vacancies, which are the dominant positron traps as isolated O vacancies are not usually expected to trap positrons). The broad and intense momentum density of the O-related electronic shells compared basically to any cation in the Periodic Table makes positrons a very sensitive probe of the local O content around vacancy defects and can potentially help to detect O vacancies when they start to complex with cation vacancies.<sup>7</sup>

### III. RECENT DEVELOPMENTS

#### A. Defects in narrow-gap semiconductors

##### 1. Germanium

Positrons are most sensitive to negatively charged and neutral vacancy defects. Defects with acceptor character are hence an optimal subject to be studied with positron annihilation spectroscopy, aiming at elucidation of compensation and passivation phenomena in *n*-type doped semiconductors. Germanium and  $\text{Ge}_{1-x}\text{Sn}_x$  alloys suffer from the difficulty of increasing doping levels above  $10^{19} \text{ cm}^{-3}$  due to efficient donor passivation. For comparison, in Si, the threshold is almost two orders of magnitude higher. The mechanisms of dopant (P, As, Sb) passivation that are intimately related to dopant diffusion in Ge and GeSn alloys have been recently studied in detail with positron annihilation spectroscopy in bulk Ge crystals as well as in thin Ge and GeSn thin films.<sup>15–19</sup> Complexes of mono-vacancies with the *n*-type dopants are the main defects observed with positron annihilation spectroscopy, while the isolated mono-vacancies in Ge are mobile well below room temperature.<sup>20</sup> Also, dopant diffusion in Ge proceeds via the vacancy mechanism.<sup>21</sup>

Figure 3 shows examples of experimental and computational Doppler broadening ratio curves for highly P-doped Ge and GeSn alloys.<sup>17–19</sup> The findings indicate that mono-vacancy complexes  $V-nP$  are responsible for the passivation of dopants in highly P-doped Ge as well as in  $\text{Ge}_{1-x}\text{Sn}_x$  alloys. The strong attraction of monovacancies toward the phosphorus atoms is the dominant dopant deactivation mechanism in P-doped Ge and  $\text{Ge}_{1-x}\text{Sn}_x$  alloys. The experiments also confirm the increase in the number of P atoms around the monovacancies with increasing P-doping. We note that similar interpretations are difficult to make in the case of As due to the indistinguishable nature of Ge and As atoms in positron annihilation characteristics; for instance, the isolated mono-vacancy and the V–As pair are indistinguishable in the calculated spectra. The main features to analyze in the ratio curves in Fig. 3 are the intensity at low momenta (*S* parameter region), the peak-like shoulder at around 1.1 a.u., and the level and slope of the intensity at high momenta (*W* parameter region). Detailed analysis of the high momentum behavior strongly suggests that there is at

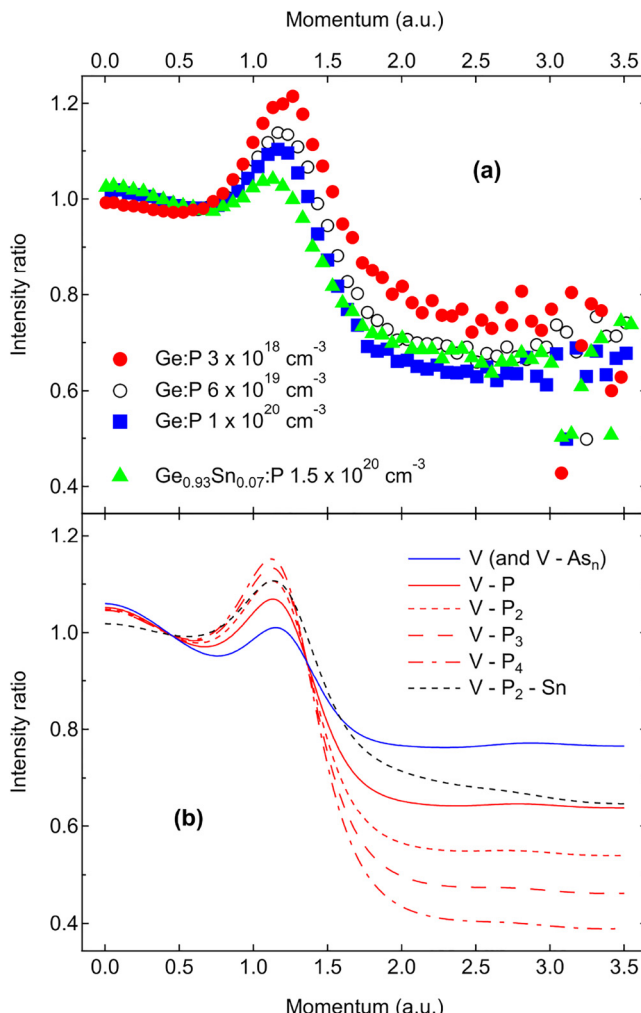


**FIG. 3.** Examples of experimental (a) and calculated (b) Doppler broadening ratio curves for Ge and GeSn alloys with vacancy defects decorated with P. The important features are the intensity in the low momentum range (below 0.5 a.u.), the shoulder/peak-like feature at around 1.0–1.5 a.u. and both the intensity and the slope at momentum values above 2 a.u. It is clearly seen that the addition of P atoms next to the mono-vacancy increases the shoulder/peak-like feature and decreases the intensity at high momenta. Addition of Sn increases the high momentum intensity and also somewhat changes the slope. Data adapted from Refs. 18 and 19.

least 1 Sn atom present around the monovacancy in the vacancy-dopant complexes in  $\text{Ge}_{1-x}\text{Sn}_x$  alloys. It is, however, important to note that the presence of a single Sn atom around the vacancy has not been found to have any remarkable effect on doping activation.

## 2. Gallium antimonide

While Ge is an elemental narrow-gap semiconductor where the fundamental native point defects are the mono-vacancy and the

self-interstitial, GaSb is a narrow-gap compound semiconductor where the number of possible native point defects is significantly higher. Mono-vacancies can occur on both sublattices, both atoms can take an interstitial position, and there is an additional class of defects where an atom occupies the wrong sublattice: antisites. GaSb exhibits two uniquely highly asymmetric properties that are related to point defects: strong propensity toward *p*-type conductivity and unusually low diffusivity of Sb that diffuses three orders of magnitude slower than Ga through the lattice.<sup>22</sup> These asymmetries are likely related to the position of the valence and conduction band edges relative to the Fermi level stabilization energy, a concept developed by W. Walukiewicz:<sup>23</sup> in GaSb, the valence band essentially coincides with this level, favoring the equilibrium formation of acceptor-type defects.<sup>24</sup>

The identity of the acceptor-type defect responsible for the *p*-type conductivity of nominally undoped GaSb was under debate for quite some time.<sup>25–28</sup> Positron annihilation experiments combined with insights from theoretical work showed recently that  $V_{\text{Ga}}$  and  $\text{Ga}_{\text{Sb}}$  are the dominant acceptor-type native defects in GaSb, but their relative importance depends on the crystallization conditions.<sup>29–31</sup> In GaSb substrate crystals, the concentration of Ga antisites is an order of magnitude higher than that of the Ga vacancies, making the antisite the main cause for *p*-type behavior. Instead, in epitaxial GaSb, the Ga vacancies play a more significant role. Note that the high concentrations of the  $\text{Ga}_{\text{Sb}}$  antisites that act as negative ion like defects from the perspective of positron annihilation experiments makes the detailed interpretation of annihilation signals challenging.

The amphoteric nature of the Sb vacancy has been proposed as the origin for the unusually slow diffusion in the Sb sublattice.<sup>22</sup> Driven by the strong propensity to form acceptor-type defects, the Sb vacancy could be unstable, easily exchanging sites with a neighboring Ga atom, resulting in a Ga vacancy and a Ga antisite. This mechanism would enhance the Ga diffusion while at the same time suppressing the diffusivity of Sb due to the lack of Sb-related defects in the lattice. Similar amphoteric behavior of point defects has been observed in, e.g., GaAs and InN.<sup>23,32</sup> Recent positron annihilation experiments confirmed this picture.<sup>33</sup> The positron lifetime experiments were performed by irradiating undoped, *p*-type GaSb with high-energy protons at 30 K with an *in situ* positron lifetime spectrometer.<sup>34</sup> The positron lifetime results show that the Sb vacancy in GaSb becomes unstable at temperatures above 150 K and undergoes a transition resulting in a Ga antisite and Ga vacancy. The activation energy for the process is estimated as  $0.6 \pm 0.1 \text{ eV}$ , which is comparable to that of the unstable Si vacancy in Si. Due to the instability of the Sb vacancy, the acceptor-type defect concentration in *p*-type GaSb is further increased as a result of irradiation.

## B. Defects in wide-gap nitride semiconductors

In *n*-type doped compound semiconductors, and, in particular, in *n*-type nitride and oxide semiconductors families that exhibit wide bandgaps, cation (metal) vacancies tend to be the acceptor-type defects with lowest formation energies predicted by calculations.<sup>35,36</sup> This is also observed in experimental work where cation vacancy defects, such as the Ga vacancy in GaN, are found

to be the dominant native compensating defect in *n*-type conditions.<sup>37,38</sup> Positron annihilation methods are most sensitive to cation vacancies in nitride and oxide semiconductors for two main reasons: (i) their acceptor character leading to a negative or at most neutral charge state, and (ii) the nitrogen/oxygen vacancies are in their isolated form too small to effectively trap a positron, even if they were in a negative charge state. In the latter case, these nitrogen/oxygen vacancies may still exhibit shallow Rydberg states, but they are then indistinguishable from negative ion-like defects.

Positron annihilation spectroscopy has been useful for identifying the main native acceptor defect in many *n*-type nitride and oxide semiconductors: the Ga vacancy in GaN, the Zn vacancy in ZnO, the In vacancy in InN.<sup>37,39,40</sup> In  $\text{In}_2\text{O}_3$ , experiments have shown that it is not the In vacancy but rather the O interstitial,<sup>41</sup> and also in AlN, it is not the Al vacancy but the identity of the dominant native acceptor defect is still unclear.<sup>10</sup> Recently, the focus of positron annihilation studies in wide-gap nitride semiconductors has shifted toward the elucidation of defect-related issues in technologically relevant InGaN and AlGaN alloys as well as opto-electronic and power electronics devices made thereof.<sup>12,42–48</sup> In addition, both fundamental and applied aspects of *p*-type doping with acceptor impurities have been investigated with positron annihilation methods.<sup>49–51</sup> As an illustrative example, it was recently found that Be impurities exhibit amphoteric behavior in GaN,<sup>6</sup> similar to what has been found for Li impurities in ZnO<sup>52,53</sup> and for certain vacancy-type defects in III–V semiconductors.<sup>33,54</sup> This behavior involves switching between substitutional (acceptor) and interstitial (donor) positions in the lattice. The amphoteric nature was observed through the dominance of  $\text{Be}_{\text{Ga}}$  in the positron annihilation signals in Be-doped GaN thin films and bulk crystals, as shown in Figs. 1(f) and 2(f). In the *S*–*W* plot [Fig. 2(f)], the data points of the Be-doped GaN samples do not fall on the line connecting the GaN lattice to  $V_{\text{Ga}}$  nor above it (nor to the right of it), as would be typical of GaN containing either in-grown or processing-induced  $V_{\text{Ga}}$ -related defects. Instead, all the data points from the Be-doped samples are located in the vicinity of the calculated points for  $\text{Be}_{\text{Ga}}$ -related defects. From the ratio curves in 1(f), it can be seen that the defects observed in Be-doped GaN sample are related to  $\text{Be}_{\text{Ga}}$ , as the ratio curves for the other defects are notably different. It is notable that despite its small associated volume,  $\text{Be}_{\text{Ga}}$  still acts as an efficient positron trap as found in Ref. 6. The calculations for neutral and negative charge states of  $\text{Be}_{\text{Ga}}$  show that the differences in the original atomic configurations are insignificant from the point of view of the positron signals due to the relaxations produced by the positron localized in the defect. Interestingly, subjecting the material to high enough temperatures drives the Be impurities to interstitial positions, observed through the emergence of  $V_{\text{Ga}}$ -related defects in concentrations comparable to those of  $\text{Be}_{\text{Ga}}$ . The thermal switching between interstitial and substitutional sites of Be appears reversible, as Be-doped GaN is predominantly semi-insulating before and after subjection to high temperatures. It is possible that this amphoteric switching is a universal property of light atom dopants substituting for heavy cations in compound semiconductors.

### 1. GaN: Ammonothermal crystals

Ammonothermal growth of GaN crystals for substrates has seen been developing strongly during the past 20 years.<sup>57</sup> Figure 4 shows

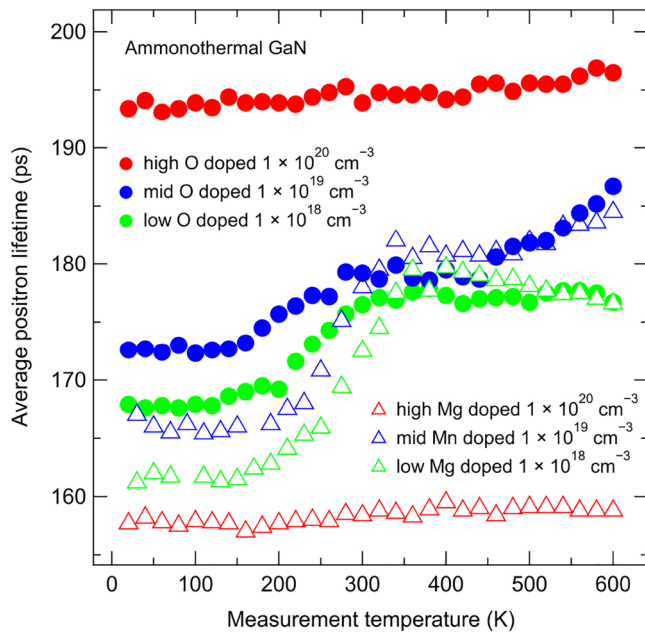


**FIG. 4.** The average positron lifetime measured as a function of temperature in differently doped ammonothermal GaN crystals. Data adapted from Refs. 55 and 56.

27 January 2024 13:37:47

the average positron lifetime, measured as a function of temperature in ammonothermal GaN crystals doped with O, Mg, or Mn at various concentrations.<sup>55,56</sup> In the highly Mg-doped crystal, no evidence of Ga vacancies is observed and the positron lifetime is that of the GaN lattice—there is slight temperature dependence originating from the thermal expansion of the lattice. The temperature behavior of the average lifetime at temperatures below 300–400 K in the moderately doped crystals is indicative of the competition between negative-ion-type defects that act as shallow positron traps for positrons and Ga vacancy defects. The high temperature behavior is different in these samples, originating from the differences in the detailed nature of the Ga vacancies. We note that the defect distributions in ammonothermal GaN crystals tend to be complex, making the decomposition of the lifetime spectra into components difficult.<sup>56</sup> This complicates the interpretations compared to a clear-cut case such as that presented for AlN in Fig. 2(b), but the temperature dependence of the data provides interesting insights.

The low temperature behavior of the average positron lifetime in the moderately doped crystals is consistent with Mn/Mg doping as well as with the residual Mg concentrations in the O doped crystals. The highest O-doped sample shows very little temperature dependence, and this is likely due to the screening of electric charge effects through the very high free electron concentration in that sample. The high temperature (above 400 K) behavior of the moderately doped crystals is different for different dopants. In the case of low Mg doping, the average lifetime decreases with increasing temperature, indicative of negatively charged Ga vacancies at concentrations of about  $1 \times 10^{17} \text{ cm}^{-3}$ . In contrast, in the other

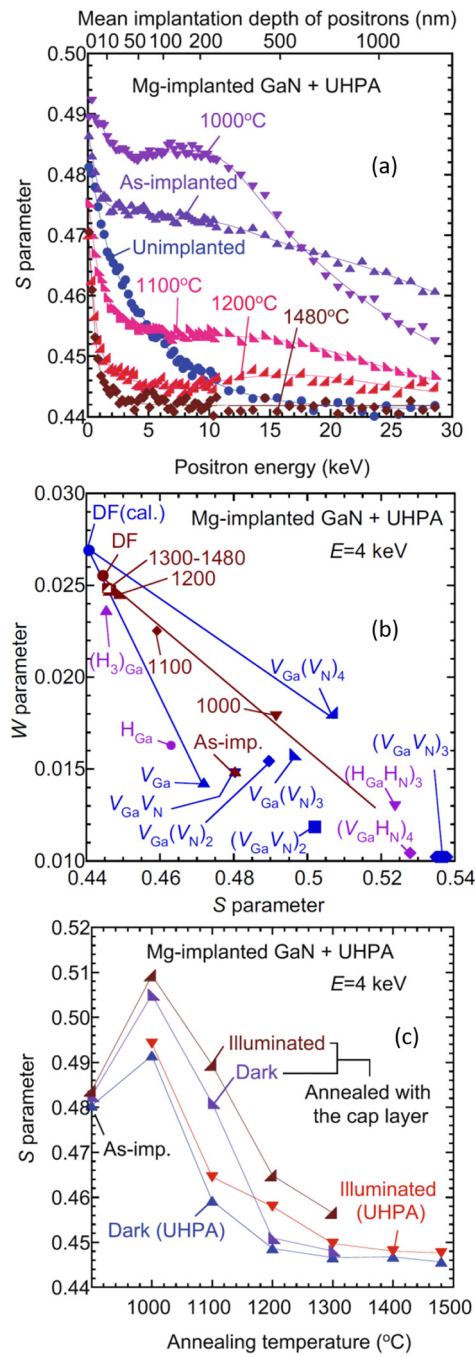


**FIG. 5.** (a) The S parameter as a function of incident positron energy E for Mg-implanted GaN before and after ultra-high-pressure annealing (UHPA). (b) Experimental (brown) and calculated (blue, purple) (S, W) values for identifying the relevant defects. (c) Annealing behavior of the S parameter for Mg-implanted GaN before and after UHPA, with and without sample illumination. Figures reproduced from Uedono *et al.*, Sci. Rep. **10**, 17349 (2020). Copyright 2020 Author(s), licensed under a Creative Commons Attribution (CC BY 4.0) license.

samples, the vacancy concentrations are much higher (above  $5 \times 10^{18} \text{ cm}^{-3}$ ), as the abrupt change of the temperature dependence at 300 K is indicative of saturation trapping. This also means that the lifetime characterizing the Ga vacancy in these samples is clearly shorter than that in typical Ga vacancies (closer to 180 ps than 235 ps). The second increase of the average lifetime above 500 K in the mid-O-doped and mid-Mn-doped crystals strongly suggests escape from the shortest-lifetime Ga vacancies and re-trapping at some larger Ga vacancies. This has been interpreted as competition between  $V_{\text{Ga}}-\text{H}$  and  $V_{\text{Ga}}-2\text{H}$  complexes.<sup>55</sup> These complexes are likely the dominant positron trap also in the highest O-doped sample. The presence of ammonia in the growth by the ammonothermal method appears to be the key to the extremely high Ga vacancy concentrations and their complexes with multiple H atoms.<sup>55,58,59</sup>

## 2. GaN: Implantation processing

Doping GaN with acceptor impurities to make it *p*-type is challenging, even if it is routinely performed employing Mg, as it requires specific thermal treatments for the activation of the acceptors. Vertical power devices require embedded *p*-type regions to suppress the electric field spreading near the edges of junctions, and ion implantation processing is a common approach for selective *p*-type doping of semiconductors. However, the removal to the detrimental effects of ion implantation in GaN requires annealing temperatures higher than the decomposition temperature of GaN. A promising approach is to employ ultra-high-pressure-annealing (UHPA) at 1 GPa N<sub>2</sub> pressure and temperature close to 1500 °C.<sup>49,60,61</sup> Figure 5 shows the positron annihilation results obtained in Mg implanted (300 nm thick box profile with  $1 \times 10^{19} \text{ cm}^{-3}$  Mg concentration) and UHPA treated GaN.<sup>49</sup> In Fig. 5(a), the creation of heavy vacancy type damage in the implanted region is seen as an increase in the S parameter. With thermal treatments with increasing temperature, the S parameter first increases and then gradually decreases and reaches the pre-implantation level at the highest temperature. The (S, W) plot in Fig. 5(b) shows that the primary damage is predominantly single  $V_{\text{Ga}}$ -type defects that form larger clusters together with N vacancies in the annealing process and gradually disappear with increasing temperature. Figure 5(c) shows also the effect of illuminating the samples with 325 nm light during experiments: the increase in the S parameter indicates that some vacancies change their charge state from positive to neutral or from neutral to negative in the implanted and annealed samples, as expected for material where the Fermi level is close to the valence band.

## 3. InGaN and AlGaN alloys

The identification of a vacancy defect in an alloyed crystalline material is cumbersome. In elemental crystals and multi-element compounds, it is a certain type of atom missing from the (sub) lattice site, but in a random alloy with multiple elements sharing the same (sub)lattice, the exact identity of the missing atom cannot be deduced from the surroundings. In addition, these surroundings are not uniquely defined. For example, in an  $\text{In}_x\text{Ga}_{1-x}\text{N}$  or  $\text{Al}_x\text{Ga}_{1-x}\text{N}$  alloy, the cation (metal) site vacancy is surrounded by 4 N atoms, but the 12 next-nearest neighbors are randomly

27 January 2024 13:37:47

distributed In and Ga atoms with the probability of occurrence of each atom defined by the average alloy composition. There are already 144 non-equivalent configurations for the In and Ga atoms in this 12-atom shell.<sup>62</sup> The characteristics of the vacancy may significantly depend on the configurations of further neighbors too. In practice, this challenge is often simply omitted and “cation” or “metal” vacancies are the subject of investigations. For N vacancies in  $In_xGa_{1-x}N$  or  $Al_xGa_{1-x}N$ , the immediate surroundings consist of four metal atoms and similar challenges, in principle, exist. It is somewhat fortuitous that the cation vacancies have very similar electrical character in GaN, InN, and AlN,<sup>63</sup> and hence, the cation vacancies in the alloys can be assumed to have similar character as well. Similar reasoning is justified for the N vacancies too.

Recently, positron annihilation spectroscopy has been more and more employed to study  $In_xGa_{1-x}N$  and  $Al_xGa_{1-x}N$  alloys with varying compositions.<sup>12,42–44,46–48,64</sup> Figure 6 shows two ( $S, W$ ) plots that highlight the challenges when analyzing experimental data from these nitride alloys. In Fig. 6(a), ( $S, W$ ) data for as-grown and irradiated molecular beam epitaxy grown  $In_{0.37}Ga_{0.63}N$  layers are shown:<sup>42</sup> the colored symbols connected by a line denote the layer (left) and the interface region (right) between  $In_xGa_{1-x}N$  and the Si substrate. The irradiations were performed with 40 and 100 keV  $He^+$  ions to combined fluences between  $5 \times 10^{12}$  and  $1 \times 10^{15} \text{ cm}^{-2}$  (for technical details, see Ref. 42). The ( $S, W$ ) points for GaN and InN lattices are shown for comparison. The dotted curve connecting the GaN and InN extremes represents the ( $S, W$ ) parameters for defect-free  $In_xGa_{1-x}N$  as a function of the indium content as shown in Ref. 65. The region in the ( $S, W$ ) plane corresponding to defect-free alloys with 37% indium is highlighted. Further, three more points, the gallium vacancy  $V_{Ga}$  in GaN, the indium vacancy  $V_{In}$ , and the indium vacancy decorated with several nitrogen vacancies  $V_{In-nV_N}$   $n \geq 2$ , both in InN, are shown.<sup>40,66</sup> The shaded region between  $V_{Ga}$  and  $V_{In}$  reflects the calculated scatter of the Doppler parameters in  $In_xGa_{1-x}N$  systems containing a metal vacancy, resulting from the atom distribution in the random alloy.<sup>65</sup> All the ( $S, W$ ) parameters are shown as normalized to the GaN reference.

In the as-grown sample, the ( $S, W$ ) values of the layer lie rather close to one of the extremes of the cation vacancy in  $In_xGa_{1-x}N$  systems [the shaded region in Fig. 6(a)]. This suggests that most positrons annihilate as trapped at cation vacancies in the sample. The right shift of data points obtained at the interface between the layer and the substrate (at higher implantation energies) in the ( $S, W$ ) plane is interpreted as the interface being rich in cation vacancies complexed with nitrogen vacancies. As seen in the figure, these  $In_xGa_{1-x}N/Si$  interface values are very close to those of  $V_{In-nV_N}$  calculated for InN indicating an increase in the number of  $V_N$  associated with a cation vacancy as shown in Ref. 40 and suggesting higher indium content in the near-interface region. With the increase of irradiation fluence, the data points in the layers converge toward the  $V_{In}$  characteristic value. Hence, either the vacancy defects are mostly created in In-rich regions, or the formation of In-rich regions is enhanced by high-fluence implantation, leading to increased positron trapping at vacancies in those regions. Despite the increasing implantation dose there is no observable change near the  $In_xGa_{1-x}N/Si$  interface where the cation vacancies already exhibit  $V_{In-nV_N}$ -like character. It is

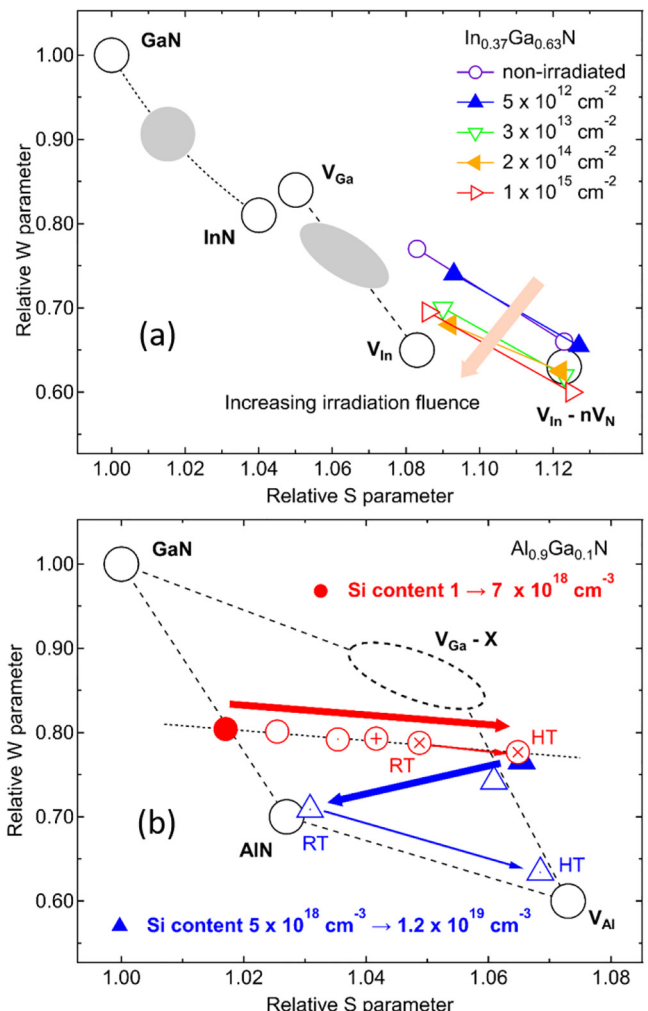


**FIG. 6.** (a) Normalized ( $S, W$ ) values in the layer (left) and close to the interface (right) measured in as-grown and irradiated InGaN alloy samples. Values expected in GaN, InN, and the vacancies therein are also shown. The gray shaded areas show the expected range of the alloy ( $S, W$ ) values. (b) Normalized ( $S, W$ ) values measured at room temperature (RT) in Si-doped AlGaN alloy samples (unless marked HT). The dashed oval marks the region of the ( $S, W$ ) parameters for ingrown  $V_{Ga}$  complexes in GaN. The thick arrows show the direction of increase of Si concentration in the samples, and the narrower arrows the trend of changing annihilation parameters as a response to increasing measurement temperature from 300 (RT) to 600 K (HT). The dashed lines connect the bulk and vacancy points in GaN and AlN, while the dotted line illustrates the trends in the AlGaN data. Data adapted from Refs. 12 and 42.

unlikely that the tendency of the layer data toward InN-like behavior would reflect preferential formation of cation vacancy defects in the regions of higher indium content in random alloys as the cation vacancy formation energy is higher in InN than in GaN.<sup>67</sup> The results hence reflect a change in the distribution of the metal atoms and indicating the generation of indium-rich regions in the  $In_xGa_{1-x}N$  lattice under heavy irradiation.

**Figure 6(b)** shows the ( $S, W$ ) parameters characterizing  $\text{Al}_{0.90}\text{Ga}_{0.10}\text{N}$  thin films  $n$ -type doped with Si. For details about sample preparation and characteristics, see Ref. 12. Characteristic points representing the GaN lattice, AlN lattice,  $V_{\text{Al}}$  in AlN, and the typical in-grown Ga vacancies in GaN (denoted by  $V_{\text{Ga-X}}$ ) are also shown. All the measured ( $S, W$ ) data fall inside the area defined by these four points. This indicates that the data measured in the AlGaN samples can be analyzed as the AlGaN alloy and corresponding cation vacancy defects. At the same time, this plot highlights the difficulty in analyzing the ( $S, W$ ) data when positrons annihilate in more than two different states in a set of samples. The data points do not necessarily form a line as in the case of exactly two states, making the detailed identification of the positron traps, as well as the determination of their concentrations, generally a very difficult task.

In **Fig. 6(b)**, the red markers show the data from AlGaN samples with the Si content at most  $7 \times 10^{18} \text{ cm}^{-3}$ . These  $S, W$  points form a straight line, indicating that these samples contain two (and only two) distinct states in which the positrons annihilate. At the left end, the ( $S, W$ ) data fall close to the line connecting GaN and AlN lattice values. Hence, the lowest doped sample represents the AlGaN alloy lattice in this sample set. At the right end of the line, with increasing Si concentration, the data points converge close to the line connecting  $V_{\text{Ga-X}}$  in GaN and  $V_{\text{Al}}$  in AlN. These data are interpreted as saturation of positron trapping at the group III (cation) vacancy defects (V<sub>III</sub>) present in most of the AlGaN samples. The trend-like shift of the ( $S, W$ ) parameters toward the vacancy-like data in these samples indicates an increase in the cation vacancy concentration with increasing Si doping. Interestingly, there is no scatter of the experimental data along the lines joining GaN and AlN, or the  $V_{\text{Ga-X}}$  in GaN and  $V_{\text{Al}}$  in AlN, indicating that all the cation vacancy defects have similar character in these samples. This also allows determining the cation vacancy concentrations in these samples, as the trapping rate  $\kappa_D$  can be evaluated from the  $S$  parameter (similarly for  $W$ , but here it is more practical to only use  $S$  as the changes in  $W$  are minimal) of each sample through  $\kappa_D = \tau_B^{-1}(S - S_B)/(S_D - S)$ . Here,  $S_B$  is there parameter characterizing the “perfect” AlGaN alloy,  $S_D$  that of the cation vacancy and  $\tau_B$  is the positron lifetime in the AlGaN lattice. The vacancy concentration  $c_D = \kappa_D/\mu_D$ , where  $\mu_D$  is the positron trapping coefficient of the vacancies. Further increase in the Si content, as shown by the behavior of the ( $S, W$ ) data with blue markers, results in a very different behavior, with the data shifting strongly to AlN-like values. This is probably related to Si DX center formation, discussed in detail in Ref. 12. We note that the measurements as a function of temperature add important insight into the interpretations as they reveal the effect of negative ion like defects competing in positron trapping with the vacancies. It is also worth noting that most of the positron annihilation studies in  $\text{In}_x\text{Ga}_{1-x}\text{N}$  and  $\text{Al}_x\text{Ga}_{1-x}\text{N}$  alloys show similar trends, that is, the omnipresence of cation vacancy–nitrogen vacancy complexes with varying sizes in this family of materials.<sup>12,42–44,46–48,64</sup>

#### 4. Interface states in device structures

The ability to study real device structures consisting of several layers containing multiple heterointerfaces with positron annihilation

allows to make direct conclusions on defects affecting device performance.<sup>45,48</sup> Polar III-nitride heterostructures provide an interesting subject for these studies as the polarization discontinuity-induced macroscopic electric field drives positrons to the same interface as hole in such a structure, causing two-dimensional spatial confinement of the positron state at that interface.<sup>5</sup> **Figure 7** shows Doppler broadening ratio curves measured in N-polar  $\text{GaN}/(\text{Al},\text{Ga})\text{N}/\text{GaN}$  structures of a high electron mobility transistor (HEMT), as well as those measured in N- and Ga-polar multi-quantum well (MQW) structures as discussed in Ref. 45. The data show that the MQW interface signal is different from that calculated for the perfect AlN/GaN interface,<sup>5</sup> and in the case of the  $(\text{Al},\text{Ga})\text{N}/\text{GaN}$  interface, it should in fact rather

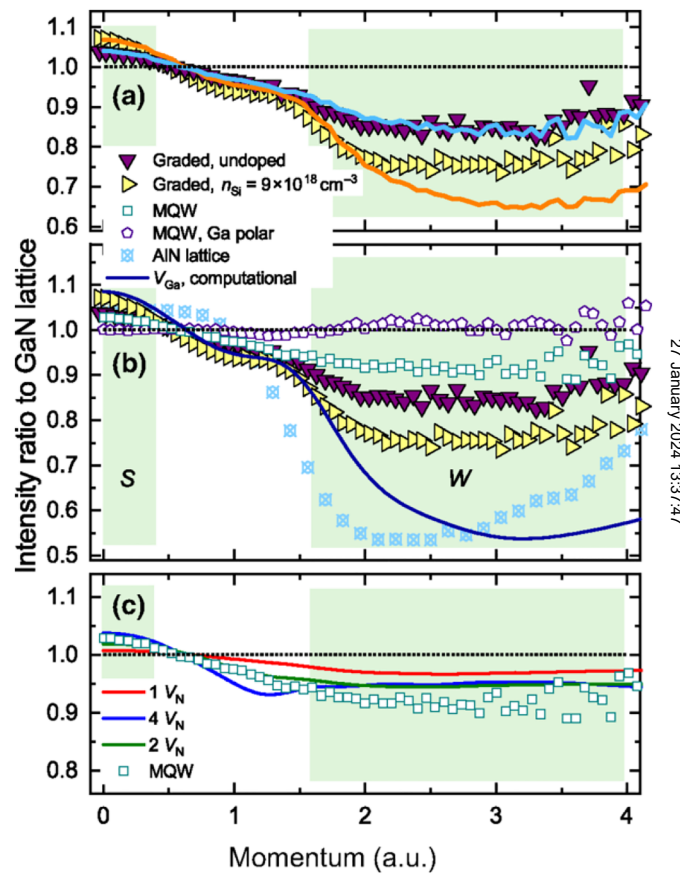


**FIG. 7.** (a) Doppler broadening ratio curves and linear combinations of N-polar MQW signal and  $V_{\text{Ga}}$  compared to doped and undoped HEMT structures. (b) Ratio curves of various heterostructures. The structures are N polar unless Ga polarity is indicated. (c) Ratio curves of the N-polar MQW sample and calculated  $V_N$  for a different number of N vacancies at the AlN/GaN interface in the supercell. The calculated curve for the AlN/GaN structure with no vacancies (not shown) is indistinguishable from the structure with  $1 V_N$ . Regions representative of the ( $S, W$ ) parameters are highlighted. Reproduced with permission from Prozheeva *et al.*, Phys. Rev. Appl. 13, 044034 (2020). Copyright (2020) the American Physical Society.

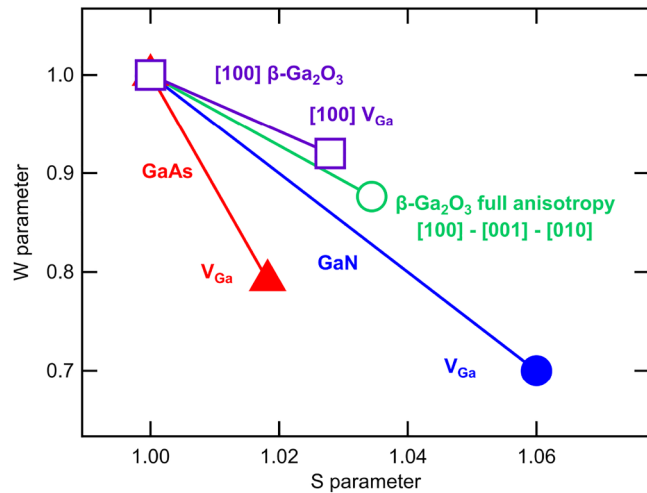
closely resemble the GaN lattice signal due to the lower fraction of Al in the system.

Figure 7(c) shows ratio curves for the MQW sample, which is shown to produce a similar signal to the bottom (Al,Ga)N/GaN interface in the N-polar HEMT structure, and theoretically calculated AlN/GaN heterostructures containing different amounts of N vacancies  $V_N$  at the interface. It is important to note that N vacancies placed elsewhere in the supercell, irrespective of whether simple GaN or AlN, or an interface structure is considered, do not trap positrons and hence do not modify the calculated annihilation signals. However, when positrons are already confined in one dimension to the interface regions, the removal of N atoms from the interface modifies the positron annihilation signals to an observable extent. Comparison of the theoretical predictions and the experimental data in Fig. 7(c) shows that positrons are trapped at open volume features involving  $V_N$  (but not  $V_{Ga}$ ) localized at the (Al,Ga)N/GaN interface. A high concentration of  $V_N$  leads to such changes in ratio curves as the increased S parameter and lower intensity at high momenta, but without the typical features of Ga vacancies. If the  $V_N$  are in the neutral charge state, as is likely in n-type material,<sup>35,68</sup> they will not modify the electric fields driving positron (or hole) confinement at the interface. Importantly, these N vacancies likely act as efficient hole traps due to their deep-donor character, directly affecting the device performance.

### C. The unusually challenging $\beta\text{-Ga}_2\text{O}_3$

Semiconducting oxides typically exhibit more complex composition and lattice structures than the simple equiatomic binary compounds such as GaN, AlN, and InN, and even their alloys. The number of different point defect configurations increases rapidly with structural complexity. For example, the bixbyite  $\text{In}_2\text{O}_3$  structure is such that the In site has two different types of adjacent empty “O sites” without any atoms missing from the lattice. In  $\beta\text{-Ga}_2\text{O}_3$ , the two Ga sites are differently coordinated with either 4 or 6 adjacent O atoms. Metal oxides with more than one metal, such as the  $\text{ABO}_3$  structured perovskites, have even more complex lattice structure and a wider variety of possible defects. In addition, it turns out that oxide semiconductors have a tendency for hosting high concentrations of a wide variety of vacancy complexes, involving both metal and oxygen vacancies. The challenge in detailed identification of point defect in the perovskite oxides and their alloys has been highlighted in several recent papers.<sup>69–73</sup> The non-trivial stoichiometry, rich distribution of point defects, and lack of well-defined reference samples all play an important role in making identification of defects challenging.

Controlling the experimental conditions such as sample temperature and illumination, as well as conducting experiments on varying samples with trends in, e.g., growth stoichiometry or doping, makes positron annihilation spectroscopy a powerful technique in vacancy defect identification. However, as very recently discovered in the case of  $\beta\text{-Ga}_2\text{O}_3$ ,<sup>74–78</sup> this is not always sufficient. Theory predicts three different low-energy “split  $V_{Ga}$ ” configurations ( $V_{Ga}^{la}$ ,  $V_{Ga}^{lb}$ , and  $V_{Ga}^{lc}$ ) where a neighboring Ga atom moves to an interstitial position halfway toward the original  $V_{Ga}$ , creating two “half-vacancies” complexed with an interstitial in between.<sup>79</sup> In addition, the Doppler broadening signals measured in  $\beta\text{-Ga}_2\text{O}_3$



**FIG. 8.** Illustration of differences in the ( $S$ ,  $W$ ) parameters of the defect-free lattice and Ga vacancy in GaAs, GaN, and  $\beta\text{-Ga}_2\text{O}_3$ . The data are shown as normalized to the respective lattice values of these materials, in the [100] direction for  $\beta\text{-Ga}_2\text{O}_3$ . The anisotropy or measurement orientation dependence of the ( $S$ ,  $W$ ) parameters in GaAs and GaN is smaller than the symbol size in the figure. In  $\beta\text{-Ga}_2\text{O}_3$ , the largest difference between the values of the lattice and vacancy, which is predicted to occur for the unrelaxed  $V_{Ga1}$  in measurement along [100], is smaller than the full measured anisotropy. It is also clearly smaller than the vacancy-lattice differences in GaAs and GaN: for both parameters in the case of GaN and for the  $W$  parameter in the case GaAs.<sup>74</sup>

27 January 2024 13:37:47

exhibit colossal anisotropy that is highly unusual in 3D semiconductor crystal lattices, as shown in Fig. 8. It is important to note that the data obtained in Doppler broadening experiments are by definition dependent on the measurement direction relative to the crystal orientation. However, when performing defect studies in “conventional” semiconductors with Doppler broadening, the measurement orientation is usually disregarded as the relative differences in the signals in the different directions are negligible. For example, in Fig. 8, the anisotropy in GaAs or GaN is smaller than the marker size.<sup>2</sup>

The colossal anisotropy has been the cause of significant issues in understanding positron annihilation results in  $\beta\text{-Ga}_2\text{O}_3$ , as the various vacancy signals and the  $\beta\text{-Ga}_2\text{O}_3$  lattice signal overlap in different measurement orientations.<sup>74</sup> In experiments, the detailed form of the anisotropy will depend on the combination of positron annihilation states present in the sample. It is hence of utmost importance to pay close attention to the measurement orientation when studying  $\beta\text{-Ga}_2\text{O}_3$  with positron annihilation spectroscopy. This colossal anisotropy has, however, also proven to be fortuitous as the lack of a proper “defect-free” reference material in the case of  $\beta\text{-Ga}_2\text{O}_3$  prevents defect identification in the conventional way of comparing lifetime signals, fingerprints in the ( $S$ ,  $W$ ) plot, and ratio curves as in the above examples. As the experimentally found anisotropies are much larger than those predicted for any other positron trapping states, the present interpretations is that most (if not all)  $\beta\text{-Ga}_2\text{O}_3$  samples studied so far contain large concentrations of split Ga vacancies, possibly complexed with

hydrogen. Recent experimental and theoretical studies suggest that the complexity of vacancy defects and their complexes in  $\beta\text{-Ga}_2\text{O}_3$  may be even higher than previously considered.<sup>80,81</sup> Interestingly, in the family of sesquioxides, these unusual features appear to be exclusive to  $\beta\text{-Ga}_2\text{O}_3$ .<sup>41,82,83</sup> The journey toward understanding the detailed defect-related phenomena in  $\beta\text{-Ga}_2\text{O}_3$  has only begun.

#### IV. OPEN QUESTIONS, FUTURE CHALLENGES, AND POSSIBLE SOLUTIONS

##### A. Controlled experiments for better identification of point defects

Positron annihilation spectroscopy is a strongly comparative technique where the detailed defect identification has traditionally relied on comparison with a well-defined reference sample of the same material that does not exhibit positron trapping at vacancies. In the case of semiconductors, such a reference is usually found by synthesizing a *p*-type sample where all—or at least the majority of—the point defects are in positive charge states and hence invisible to positrons. For many novel semiconductors, in particular, oxides, such material does not exist, making the defect identification extremely difficult. Controlling the synthesis conditions, such as stoichiometry, temperature, or doping level, affects the final defect distribution in the samples via thermodynamic and kinetic processes. Controlling and tuning the experimental conditions during measurements of positron lifetime and Doppler broadening, such as sample temperature or sub-bandgap illumination conditions, has allowed more detailed analysis of charge states and opto-electronic transition levels in the bandgap.<sup>9,39</sup> Above bandgap illumination has been used to affect the band bending near the surface and change the charge states of defects for improving the selective sensitivity.<sup>49</sup> Biasing a thin film sample can be employed for the same purpose. Recently, transient experiments where sub-bandgap illumination and biasing have been employed in pump-probe mode have been used to elucidate the dynamics of charge trapping and emission processes in semiconductors,<sup>11,84</sup> but these type of experiments have not become more common. However, for identifying defects in the ever more complex lattice the experimental sophistication needs to be maximized. We strongly urge the community to adopt all advances that have been made and also devise novel approaches. Employing spin-polarized positron beams for characterizing semiconductor defects<sup>85,86</sup> is an approach that certainly merits further development. Figure 9 shows an example of a differential Doppler broadening spectrum  $N_+(p) - N_-(p)$ , where the subscripts + and – denote positive and negative magnetic fields, respectively, with respect to the positron spin polarization. The GaN sample in that study was implanted with Gd to a high fluence, and the data interpreted as positrons annihilation in vacancy clusters that are spin polarized and may be the source of ferromagnetism in that material.

Improving the selectivity of the positron annihilation signals would strongly benefit studying alloyed systems as well as complex lattice structures with several inequivalent lattice sites. Employing different illumination, electric and magnetic fields for selective defect excitation is important. It should also be considered whether the characteristic X-rays emitted after positron annihilation with core electrons could be used for direct specification of the origin of

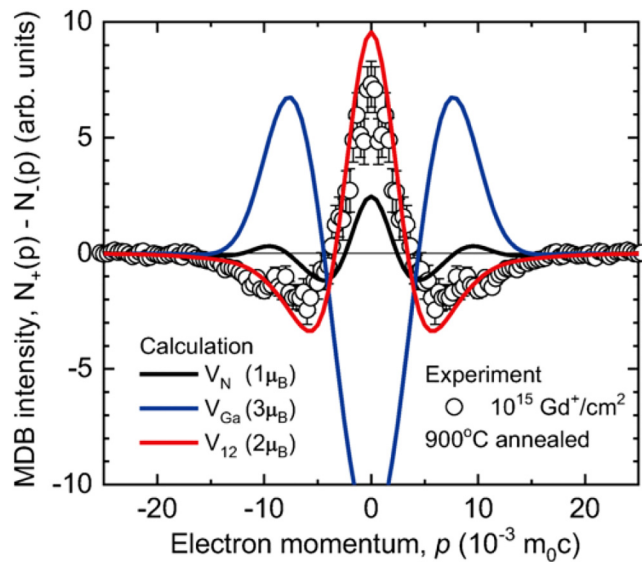


**FIG. 9.** Magnetic differential Doppler broadening spectrum measured in a Gd-implanted GaN sample. The solid curves denote the theoretical calculations assuming  $V_N$  (black),  $V_{\text{Ga}}$  (blue), and  $V_{12}$  (red) cluster. Reproduced with permission from Maekawa *et al.*, Phys. Rev. B **102**, 054427 (2020). Copyright (2020) the American Physical Society.

the annihilation signal. Measurements of  $\gamma$  rays and X-rays in coincidence should not be an obstacle. Finally, we note that when identifying defects, many early interpretations that are made in novel semiconductors are based—or at least inspired—by rules of thumb that date back to the era of defect studies Si and GaAs. However, when studying highly mismatched compounds such as semiconducting nitrides and oxides, it often turns out that defects behave unexpectedly, typically due to the wide bandgaps compared with the “traditional” semiconductors. The more complex electronic and atomic structure, the more there is variety in the defects and their character.

##### B. Beyond point defects

Positron annihilation spectroscopy is at its best when identifying and quantifying vacancy-type defects, that is point defects with open volume that are able to trap positrons into deep states and modify the annihilation characteristics. The sensitivity is at its best with mono-vacancy-sized defects and their immediate surroundings, e.g., vacancy–impurity pairs, or, in the case of the highly mismatched systems of nitrides and oxides, also cation vacancy–(multi-)nitrogen vacancy complexes. When the size of the vacancy defect (number of missing atoms) increases, the sensitivity to the exact size and structure is rapidly lost. Negatively charged defects without (or with very small) open volume are detected when they compete with vacancy defects in positron trapping but due to the large spatial extent of the Rydberg state the annihilation characteristics are the same as in the “defect-free” lattice. Determining the identity of these negative ion type defects requires comparison

with, e.g., secondary ion mass spectrometry (SIMS) for impurities. It is important to note that the total concentrations of negatively charged defects obtained from temperature-dependent positron experiments match very well those determined from temperature-dependent Hall experiments.

The sensitivity of positron annihilation to larger-scale atomic structures, such as dislocations, stacking faults, heterointerfaces, or inclusions, is not as strong as for vacancy defects. An open-core dislocation may trap a positron into a quasi-one-dimensional state, but it will be difficult to distinguish such a state from a simple vacancy defect. On the other hand, a dislocation line with associated negative charge will produce similar annihilation characteristics as negative ions. A stacking fault or a hetero-interface may be energetically favorable for a positron to trap inside either due to polarization induced electric fields or positron affinity [see Fig. 1(d)], but also in these cases the extent of the positron wave function is large enough to be indistinguishable from the surroundings or a linear combination thereof. Excess open volume in such as structure may alter the annihilation signals and even provide a means to detect N vacancies in nitrides, similarly as discussed for the GaN/AlGaN interface above. No direct evidence of positron localization inside nanoscale clusters in the semiconductor matrix has been found, but quantum-dot-like states have been found in metals<sup>88</sup> suggesting that similar phenomena could in principle be observed in semiconductors as well. Positrons are as easily injected into semiconductor devices as into single semiconductor layers, providing an excellent opportunity for employing positron annihilation spectroscopy in device structures. The recent examples<sup>45,48</sup> are promising and call for further detailed studies of defects controlling or limiting device performance.

Finally, there is a very recent development with high potential for studying 2D materials with positrons.<sup>87</sup> It should be noted that generally, a mono-layer of a material on top of a substrate is inaccessible to defect spectroscopy based on positron annihilation, while other positron-induced experiments are viable (positron Auger spectroscopy, reflection high energy positron diffraction). This limitation is due to the positron easily diffusing after thermalization and annihilating also in the substrate. Figure 10 shows the top-gate voltage scans of the resistance of a graphene transistor exposed to positrons. The middle part of the figure shows the accumulation of positive charge that results in the buildup of a positive voltage, causing a shift over time in the top-gate Dirac peak position. This result demonstrates the potential of a high-mobility graphene field-effect transistor as a probe for positron charging effects, and its use in studying positron transport, confinement, and dynamics. Correlating the charge detection with annihilation  $\gamma$ -ray detection will allow to localize the origin of annihilation and may lead to the possibility of identifying defects in 2D materials.

### C. Future developments in theoretical methods

All in all, density functional calculations of positron states and annihilation are very practical with today's computing resources and work remarkably well for crystalline solids and relatively small open volume defects such as monovacancies and vacancy clusters with at most a few missing atoms. In case of larger vacancy clusters when the predicted lifetime starts to approach  $\tau = 400$  ps, comparison

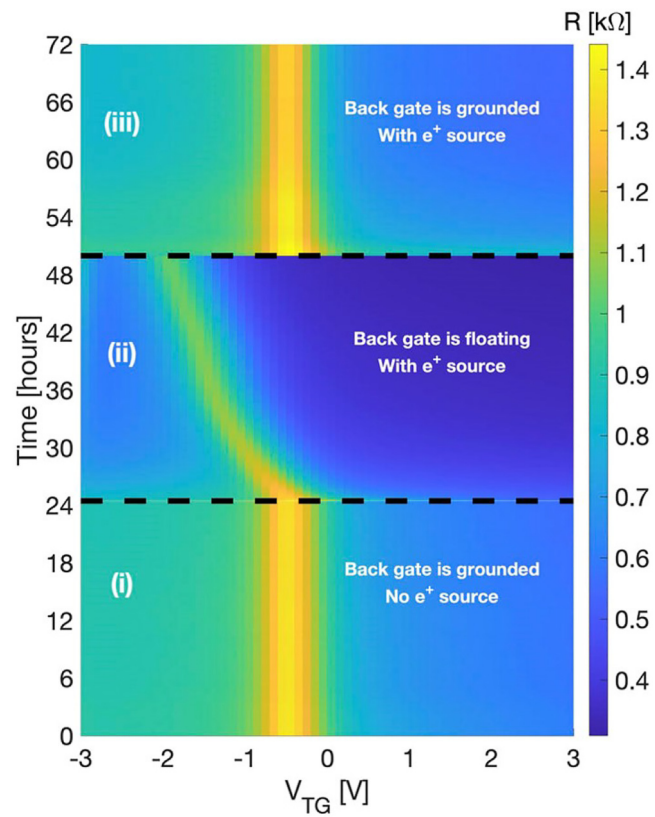


**FIG. 10.** Top-gate voltage scans of a graphene transistor as a function of time. In the measurement shown in (i), the top-gate is repeatedly scanned while keeping the back-gate grounded without exposure to positrons. The location of the Dirac peak remains stable and does not change over time. After  $\sim 24$  h (ii), a  $^{22}\text{Na}$  positron source was placed in the vacuum chamber in close proximity to the device, and the device switched to the accumulation mode, allowing the BG to float by opening the relay. Accumulated positive charge on the BG shifts the Dirac peak position over time. At a final stage (iii), the back-gate is discharged by re-connecting it to ground. The Dirac peak regains its initial position and remains stable for 24 more hours. Figure reproduced with permission from Or *et al.*, Rev. Sci. Instrum. **93**, 015002 (2022). Copyright 2022 AIP Publishing LLC.

27 January 2024 13:37:47

with experiments starts to be less straightforward and potentially even debatable, as the mechanism for the saturation of the lifetime as a function of the defect's open volume in typical models such as the local-density approximation is based on the built-in  $\tau = 480$  ps low-density limit corresponding to the negative positronium ion in vacuum, which in most case is not the physical reality. Local and semi-local models are lacking also the non-local correlation effects (image potential) experienced by the positrons on surfaces, but instead, the positrons want to escape in the vacuum in the simulations. These complications, the interest to better apply positrons to two-dimensional materials and surface systems, as well as the dependence of the technique and experiment-theory comparison on suitable defect-free reference samples, which do not exist for all interesting novel materials, necessitate the development of more

predictive methods including non-local correlations and possibly modeling them directly instead of relying on local and semilocal parametrizations only and approximating positron annihilation rate as momentum density of annihilating pairs with the help of parameterized functionals.

Recent advances in computer codes for the electronic structure problem and the development of ever faster computers have made true many-body quantum mechanics methods a viable approach to possibly even replace density-functional calculations in the future.

For crystalline solids, a method has lately shown promise for defect-free solids and can possibly be applied to vacancy defect systems in the near future is quantum Monte Carlo (QMC). For the homogenous electron–positron gas<sup>89</sup> and molecule–positron systems,<sup>90</sup> there exists already work from the past decades, but for real solids, it is important to really consider inhomogeneous systems. Simula *et al.*, used successfully variational and diffusion QMC to model positron lifetimes in crystalline solids.<sup>91</sup> Variational QMC was able to provide excellent Doppler broadening results for Si and AlN.<sup>92</sup> The same methods can be used to study the electronic structure of point defect systems such as the negative nitrogen-vacancy center in diamond,<sup>93</sup> which means that QMC studies of positrons localized at vacancy defects and direct collaboration of experiment and many-body theory can be possible in the near future. The better predictive power of the simulations will be important for novel materials systems such as metal oxides, for which defect-free reference samples usually providing the baseline for experiment-theory comparisons, are not easily available. Large vacancies and voids as well as surface studies with positrons, where the non-local electron–positron correlations are important, will be another important application of QMC and other many-body methods. In addition to QMC, any flavor of many-body theory such as many-body perturbation theory (see, e.g., Ref. 94) can potentially be generalized to treat positrons in periodic solids.

Recently, Callewaert and co-workers<sup>95,96</sup> have made an important contribution by reviving the so-called weighted density approximation (WDA), which in the positron context was originally tailored for the positron surface states.<sup>97,98</sup> WDA is basically a density functional that also can approximate non-local correlations and bind a positron in a surface state. It is a computationally cheaper alternative to many-body methods, but recent applications to solid-state systems have revealed that the original method as such does not work for predicting the annihilation properties such as positron lifetime. It turns out that in a solid-state environment it is necessary to modify the associated sum rule (loosely speaking the electronic charge,  $Q$ , assumed to screen the positron, from its default value  $Q = 1$ ),<sup>95</sup> which then unfortunately becomes a free (materials-dependent) parameter. Yang *et al.*<sup>99</sup> considered both the positron lifetime and Doppler broadening for vacancy defects in W, and noticed also that the optimum value  $Q$  for a given materials system also depends on the quantity of interest. Further development of WDA and other completely novel parameter-free, non-local correlation methods could be a viable and cheaper alternative to many-body methods and future development of these ideas would be a valuable contribution to the field.

Positron lifetime experiments and the decomposition of the experimental spectrum combined with the kinetic trapping model can be used to obtain estimates for the vacancy concentration within

the sensitivity range of the technique (around  $10^{16}$ – $10^{19} \text{ cm}^{-3}$  depending a bit on the charge state of the trap). The positron trapping rate in the kinetic equations is proportional to the vacancy concentration. Experimentally, it has been possible to confirm the proportionality constant (the so-called trapping coefficient) by correlating positron measurements and temperature-dependent Hall measurements.<sup>38,39</sup> However, currently, we are lacking the theoretical understanding of how the trapping coefficient for a given defect and charge state depends on the material, defect, and charge state in question. This information would help experimentalists to obtain more reliable absolute concentrations and understand the relative sensitivity of positron to different vacancy defects in the same system. In order to be able to model these rates, one has to first understand the processes potentially involved in positron trapping in semiconductors and insulators, and in which way and how fast the positron binding energy of  $\sim 1 \text{ eV}$  is dissipated in each possible mechanism and then focus on the most potential ones. The current understanding<sup>8</sup> relies on a simple model and there is no possibility to provide material and defect specific predictions. Recently, there has been progress in the ability model processes related to charge carrier trapping and recombination mechanisms such as defect luminescence,<sup>100</sup> non-radiative carrier capture with multiphonon emission,<sup>101</sup> radiative carrier capture,<sup>102</sup> and trap-assisted non-radiative Auger–Meitner recombination.<sup>103</sup> It is worthwhile to consider the connection of these mechanisms to the case of positron trapping to defects in semiconductors and insulators systems and generalize the ideas to two-component electron–positron density functional calculations.

Regarding the perspectives of theory and modeling in defect identification using positron annihilation, we can conclude that close collaboration with and involvement in the electronic structure and many-body theory communities is the key to success and future developments!

27 January 2024 13:37:47

## V. SUMMARY

Positron annihilation spectroscopy is a highly suitable method for studying negatively charged and neutral vacancy-type defects in semiconductors in the concentration range  $10^{15}$ – $10^{19} \text{ cm}^{-3}$ . The vacancy defects can be identified, their concentrations determined, and the physical characteristics analyzed, including formation energies, migration barriers, and optical and electrical transitions. Negatively charged defects without open volume, such as ionized acceptor impurities, also trap positron to shallow Rydberg states and can be studied at low temperatures when they compete with vacancy defects in positron trapping. The trapping and annihilation process of positrons does not depend on the conductivity or the bandgap of the semiconductor. In this Perspective, we reviewed selected examples where detailed insights on vacancy defects are obtained in narrow-gap and wide-gap semiconductors. Future advances have the potential to allow detailed studies also in semiconductors with complex lattice structures and in electronic devices.

## AUTHOR DECLARATIONS

### Conflict of Interest

The authors have no conflicts to disclose.

**Author Contributions**

**Ilja Makkonen:** Conceptualization (equal); Writing – original draft (supporting); Writing – review & editing (equal). **Filip Tuomisto:** Conceptualization (equal); Writing – original draft (lead); Writing – review & editing (equal).

**DATA AVAILABILITY**

Data sharing is not applicable to this article as no new data were created or analyzed in this study.

**ACKNOWLEDGMENTS**

This material is based upon work supported by the Air Force Office of Scientific Research under award numbers FA8655-22-1-7037 and FA8655-23-1-7057. This work has been partially supported by Finnish Cultural Foundation through the Additional Million-euro Funding to Science programme.

**REFERENCES**

- <sup>1</sup>C. Freysoldt, B. Grabowski, T. Hickel, J. Neugebauer, G. Kresse, A. Janotti, and C. G. Van de Walle, “First-principles calculations for point defects in solids,” *Rev. Mod. Phys.* **86**, 253–305 (2014).
- <sup>2</sup>F. Tuomisto and I. Makkonen, “Defect identification in semiconductors with positron annihilation: Experiment and theory,” *Rev. Mod. Phys.* **85**, 1583–1631 (2013).
- <sup>3</sup>R. Krause-Rehberg and H. S. Leipner, *Positron Annihilation in Semiconductors: Defect Studies* (Springer, 1999), Vol. 127.
- <sup>4</sup>P. J. Schultz and K. G. Lynn, “Interaction of positron beams with surfaces, thin films, and interfaces,” *Rev. Mod. Phys.* **60**, 701–779 (1988).
- <sup>5</sup>I. Makkonen, A. Snicker, M. J. Puska, J.-M. Mäki, and F. Tuomisto, “Positrons as interface-sensitive probes of polar semiconductor heterostructures,” *Phys. Rev. B* **82**, 041307 (2010).
- <sup>6</sup>F. Tuomisto, V. Prozheeva, I. Makkonen, T. H. Myers, M. Bockowski, and H. Teisseire, “Amphoteric Be in GaN: Experimental evidence for switching between substitutional and interstitial lattice sites,” *Phys. Rev. Lett.* **119**, 196404 (2017).
- <sup>7</sup>I. Makkonen, E. Korhonen, V. Prozheeva, and F. Tuomisto, “Identification of vacancy defect complexes in transparent semiconducting oxides ZnO, In<sub>2</sub>O<sub>3</sub> and SnO<sub>2</sub>,” *J. Phys.: Condens. Matter* **28**, 224002 (2016).
- <sup>8</sup>M. J. Puska, C. Corbel, and R. M. Nieminen, “Positron trapping in semiconductors,” *Phys. Rev. B* **41**, 9980–9993 (1990).
- <sup>9</sup>J.-M. Mäki, F. Tuomisto, C. J. Kelly, D. Fisher, and P. M. Martineau, “Properties of optically active vacancy clusters in type IIa diamond,” *J. Phys.: Condens. Matter* **21**, 364216 (2009).
- <sup>10</sup>J.-M. Mäki, I. Makkonen, F. Tuomisto, A. Karjalainen, S. Suihkonen, J. Räisänen, T. Y. Chemekova, and Y. N. Makarov, “Identification of the V<sub>Al</sub>-O<sub>N</sub> defect complex in AlN single crystals,” *Phys. Rev. B* **84**, 081204 (2011).
- <sup>11</sup>J.-M. Mäki, F. Tuomisto, A. Varpula, D. Fisher, R. U. A. Khan, and P. M. Martineau, “Time dependence of charge transfer processes in diamond studied with positrons,” *Phys. Rev. Lett.* **107**, 217403 (2011).
- <sup>12</sup>I. Prozheev, F. Mehinke, T. Wernicke, M. Kneissl, and F. Tuomisto, “Electrical compensation and cation vacancies in Al rich Si-doped AlGaN,” *Appl. Phys. Lett.* **117**, 142103 (2020).
- <sup>13</sup>U. Ackermann, W. Egger, P. Sperr, B. Löwe, L. Ravelli, G. Kögel, G. Dollinger, and O. Jagutzki, “Development of a new time and position resolving detector for the pulsed low energy positron system PLEPS,” *J. Phys.: Conf. Ser.* **443**, 012095 (2013).
- <sup>14</sup>E. Boroński and R. M. Nieminen, “Electron-positron density-functional theory,” *Phys. Rev. B* **34**, 3820–3831 (1986).
- <sup>15</sup>J. Kujala, T. Südkamp, J. Slotte, I. Makkonen, F. Tuomisto, and H. Bracht, “Vacancy-donor complexes in highly *n*-type Ge doped with As, P and Sb,” *J. Phys.: Condens. Matter* **28**, 335801 (2016).
- <sup>16</sup>T. Kalliovaara, J. Slotte, I. Makkonen, J. Kujala, F. Tuomisto, R. Milazzo, G. Impellizzeri, G. Fortunato, and E. Napolitani, “Electrical compensation via vacancy-donor complexes in arsenic-implanted and laser-annealed germanium,” *Appl. Phys. Lett.* **109**, 182107 (2016).
- <sup>17</sup>A. Vohra, A. Khanam, J. Slotte, I. Makkonen, G. Pourtois, R. Loo, and W. Vandervorst, “Evolution of phosphorus-vacancy clusters in epitaxial germanium,” *J. Appl. Phys.* **125**, 025701 (2019).
- <sup>18</sup>A. Vohra, A. Khanam, J. Slotte, I. Makkonen, G. Pourtois, C. Porret, R. Loo, and W. Vandervorst, “Heavily phosphorus doped germanium: Strong interaction of phosphorus with vacancies and impact of tin alloying on doping activation,” *J. Appl. Phys.* **125**, 225703 (2019).
- <sup>19</sup>A. Khanam, A. Vohra, J. Slotte, I. Makkonen, R. Loo, G. Pourtois, and W. Vandervorst, “A demonstration of donor passivation through direct formation of V-Asi complexes in As-doped Ge<sub>1-x</sub>Sn<sub>x</sub>,” *J. Appl. Phys.* **127**, 195703 (2020).
- <sup>20</sup>J. Slotte, S. Kilpeläinen, F. Tuomisto, J. Räisänen, and A. N. Larsen, “Direct observations of the vacancy and its annealing in germanium,” *Phys. Rev. B* **83**, 235212 (2011).
- <sup>21</sup>E. Hüger, U. Tietze, D. Lott, H. Bracht, D. Bougeard, E. E. Haller, and H. Schmidt, “Self-diffusion in germanium isotope multilayers at low temperatures,” *Appl. Phys. Lett.* **93**, 162104 (2008).
- <sup>22</sup>H. Bracht, S. P. Nicols, W. Walukiewicz, J. P. Silveira, F. Briones, and E. E. Haller, “Large disparity between gallium and antimony self-diffusion in gallium antimonide,” *Nature* **408**, 69–72 (2000).
- <sup>23</sup>W. Walukiewicz, “Mechanism of Schottky barrier formation: The role of amphoteric native defects,” *J. Vacuum Sci. Technol. B* **5**, 1062–1067 (1987).
- <sup>24</sup>K. Alberti and M. Scarpulla, “Suppression of compensating native defect formation during semiconductor processing via excess carriers,” *Sci. Rep.* **6**, 27954 (2016).
- <sup>25</sup>I. Poole, M. E. Lee, I. R. Cleverley, A. R. Peaker, and K. E. Singer, “Deep donors in GaSb grown by molecular beam epitaxy,” *Appl. Phys. Lett.* **57**, 1645–1647 (1990).
- <sup>26</sup>S. Dannefaer, W. Puff, and D. Kerr, “Positron line-shape parameters and lifetimes for semiconductors: Systematics and temperature effects,” *Phys. Rev. B* **55**, 2182–2187 (1997).
- <sup>27</sup>C. C. Ling, M. K. Lui, S. K. Ma, X. D. Chen, S. Fung, and C. D. Beling, “Nature of the acceptor responsible for *p*-type conduction in liquid encapsulated Czochralski-grown undoped gallium antimonide,” *Appl. Phys. Lett.* **85**, 384–386 (2004).
- <sup>28</sup>V. Virkkala, V. Havu, F. Tuomisto, and M. J. Puska, “Native point defect energetics in GaSb: Enabling *p*-type conductivity of undoped GaSb,” *Phys. Rev. B* **86**, 144101 (2012).
- <sup>29</sup>N. Segercrantz, J. Slotte, I. Makkonen, J. Kujala, F. Tuomisto, Y. Song, and S. Wang, “Point defect balance in epitaxial GaSb,” *Appl. Phys. Lett.* **105**, 082113 (2014).
- <sup>30</sup>J. Kujala, N. Segercrantz, F. Tuomisto, and J. Slotte, “Native point defects in GaSb,” *J. Appl. Phys.* **116**, 143508 (2014).
- <sup>31</sup>N. Segercrantz, I. Makkonen, J. Slotte, J. Kujala, T. D. Veal, M. J. Ashwin, and F. Tuomisto, “Increased *p*-type conductivity in GaN<sub>x</sub>Sb<sub>1-x</sub>: experimental and theoretical aspects,” *J. Appl. Phys.* **118**, 085708 (2015).
- <sup>32</sup>F. Tuomisto, A. Pelli, K. M. Yu, W. Walukiewicz, and W. J. Schaff, “Compensating point defects in <sup>4</sup>He<sup>+</sup>-irradiated InN,” *Phys. Rev. B* **75**, 193201 (2007).
- <sup>33</sup>N. Segercrantz, J. Slotte, F. Tuomisto, K. Mizohata, and J. Räisänen, “Instability of the Sb vacancy in GaSb,” *Phys. Rev. B* **95**, 184103 (2017).
- <sup>34</sup>S. Väyrynen, P. Pusa, P. Sane, P. Tikkanen, J. Räisänen, K. Kuitunen, F. Tuomisto, J. Häkkinen, I. Kassamakov, E. Tuominen, and E. Tuovinen, “Setup for irradiation and characterization of materials and Si particle detectors at cryogenic temperatures,” *Nuclear Instrum. Methods Phys. Res., Sec. A* **572**, 978–984 (2007).

27 January 2024 13:37:47

- <sup>35</sup>J. L. Lyons and C. Van de Walle, "Computationally predicted energies and properties of defects in GaN," *npj Comput. Mater.* **3**, 12 (2017).
- <sup>36</sup>J. L. Lyons, J. B. Varley, D. Steiauf, A. Janotti, and C. G. Van de Walle, "First-principles characterization of native-defect-related optical transitions in ZnO," *J. Appl. Phys.* **122**, 035704 (2017).
- <sup>37</sup>K. Saarinen, T. Laine, S. Kuusma, J. Nissilä, P. Hautajarvi, L. Dobrzynski, J. M. Baranowski, K. Pakula, R. Stepniewski, M. Wojidak, A. Wysmolek, T. Suski, M. Leszczynski, I. Grzegory, and S. Porowski, "Observation of native Ga vacancies in GaN by positron annihilation," *Phys. Rev. Lett.* **79**, 3030–3033 (1997).
- <sup>38</sup>J. Oila, J. Kivioja, V. Ranki, K. Saarinen, D. C. Look, R. J. Molnar, S. S. Park, S. K. Lee, and J. Y. Han, "Ga vacancies as dominant intrinsic acceptors in GaN grown by hydride vapor phase epitaxy," *Appl. Phys. Lett.* **82**, 3433–3435 (2003).
- <sup>39</sup>F. Tuomisto, V. Ranki, K. Saarinen, and D. C. Look, "Evidence of the Zn vacancy acting as the dominant acceptor in *n*-type ZnO," *Phys. Rev. Lett.* **91**, 205502 (2003).
- <sup>40</sup>C. Rauch, I. Makkonen, and F. Tuomisto, "Identifying vacancy complexes in compound semiconductors with positron annihilation spectroscopy: A case study of inn," *Phys. Rev. B* **84**, 125201 (2011).
- <sup>41</sup>E. Korhonen, F. Tuomisto, O. Bierwagen, J. S. Speck, and Z. Galazka, "Compensating vacancy defects in Sn- and Mg-doped In<sub>2</sub>O<sub>3</sub>," *Phys. Rev. B* **90**, 245307 (2014).
- <sup>42</sup>V. Prozheeva, I. Makkonen, R. Cuscó, L. Artús, A. Dadgar, F. Plazaola, and F. Tuomisto, "Radiation-induced alloy rearrangement in In<sub>x</sub>Ga<sub>1-x</sub>N," *Appl. Phys. Lett.* **110**, 132104 (2017).
- <sup>43</sup>S. F. Chichibu, K. Kojima, A. Uedono, and Y. Sato, "Defect-resistant radiative performance of *m*-plane immiscible Al<sub>1-x</sub>In<sub>x</sub>N epitaxial nanostructures for deep-ultraviolet and visible polarized light emitters," *Adv. Mater.* **29**, 1603644 (2017).
- <sup>44</sup>S. Ishibashi, A. Uedono, H. Kino, T. Miyake, and K. Terakura, "Computational study of positron annihilation parameters for cation mono-vacancies and vacancy complexes in nitride semiconductor alloys," *J. Phys.: Condens. Matter* **31**, 475401 (2019).
- <sup>45</sup>V. Prozheeva, I. Makkonen, H. Li, S. Keller, U. K. Mishra, and F. Tuomisto, "Interfacial N vacancies in GaN/(Al<sub>x</sub>Ga<sub>1-x</sub>)N/GaN heterostructures," *Phys. Rev. Appl.* **13**, 044034 (2020).
- <sup>46</sup>S. F. Chichibu, H. Miyake, and A. Uedono, "Impacts of Si-doping on vacancy complex formation and their influences on deep ultraviolet luminescence dynamics in Al<sub>x</sub>Ga<sub>1-x</sub>N films and multiple quantum wells grown by metalorganic vapor phase epitaxy," *Jpn. J. Appl. Phys.* **61**, 050501 (2022).
- <sup>47</sup>M. Sumiya, O. Goto, Y. Takahara, Y. Imanaka, L. Sang, N. Fukuhara, T. Konno, F. Horikiri, T. Kimura, A. Uedono, and H. Fujikura, "Fabrication of AlGaN/GaN heterostructures on halide vapor phase epitaxy AlN/SiC templates for high electron mobility transistor application," *Jpn. J. Appl. Phys.* **62**, 085501 (2023).
- <sup>48</sup>A. Uedono, Y. Kimura, T. Hoshii, K. Kakushima, M. Sumiya, M. Tsukui, K. Miyano, I. Mizushima, T. Yoda, and K. Tsutsui, "Vacancy-type defects in AlInN/AlN/GaN structures probed by monoenergetic positron beam," *J. Appl. Phys.* **133**, 225301 (2023).
- <sup>49</sup>A. Uedono, H. Sakurai, T. Narita, K. Sierakowski, M. Bockowski, J. Suda, S. Ishibashi, S. F. Chichibu, and T. Kachi, "Effects of ultra-high-pressure annealing on characteristics of vacancies in Mg-implanted GaN studied using a monoenergetic positron beam," *Sci. Rep.* **10**, 17349 (2020).
- <sup>50</sup>A. Uedono, H. Sakurai, J. Uzuhashi, T. Narita, K. Sierakowski, S. Ishibashi, S. F. Chichibu, M. Bockowski, J. Suda, T. Ohkubo, N. Ikarashi, K. Hono, and T. Kachi, "Effect of ultra-high-pressure annealing on defect reactions in ion-implanted GaN studied by positron annihilation," *Phys. Status Solidi B* **259**, 2200183 (2022).
- <sup>51</sup>T. Narita, A. Uedono, and T. Kachi, "Effects of hydrogen incorporation on Mg diffusion in GaN-doped with Mg ions via ultra-high-pressure annealing," *Phys. Status Solidi B* **259**, 2200235 (2022).
- <sup>52</sup>K. M. Johansen, A. Zubia, I. Makkonen, F. Tuomisto, P. T. Neuvonen, K. E. Knutson, E. V. Monakov, A. Y. Kuznetsov, and B. G. Svensson, "Identification of substitutional Li in *n*-type ZnO and its role as an acceptor," *Phys. Rev. B* **83**, 245208 (2011).
- <sup>53</sup>K. M. Johansen, A. Zubia, F. Tuomisto, E. V. Monakov, A. Y. Kuznetsov, and B. G. Svensson, "H passivation of Li on Zn-site in ZnO: Positron annihilation spectroscopy and secondary ion mass spectrometry," *Phys. Rev. B* **84**, 115203 (2011).
- <sup>54</sup>W. Walukiewicz, "Amphoteric native defects in semiconductors," *Appl. Phys. Lett.* **54**, 2094–2096 (1989).
- <sup>55</sup>F. Tuomisto, T. Kuittilen, M. Zajac, R. Doradziński, and D. Wasik, "Vacancy-hydrogen complexes in ammonothermal GaN," *J. Cryst. Growth* **403**, 114–118 (2014), 8th International Workshop on Bulk Nitrides Semiconductors (IWBN VIII).
- <sup>56</sup>T. Heikkilä, J. Pavlov, T. Ceponis, E. Gaubas, M. Zajac, and F. Tuomisto, "Effect of Mn and Mg dopants on vacancy defect formation in ammonothermal GaN," *J. Cryst. Growth* **547**, 125803 (2020).
- <sup>57</sup>K. Grabianska, R. Kucharski, A. Puchalski, T. Sochacki, and M. Bockowski, "Recent progress in basic ammonothermal GaN crystal growth," *J. Cryst. Growth* **547**, 125804 (2020).
- <sup>58</sup>S. Suihkonen, S. Pimpalkar, S. Sintonen, and F. Tuomisto, "Defects in single crystalline ammonothermal gallium nitride," *Adv. Electron. Mater.* **3**, 1600496 (2017).
- <sup>59</sup>A. Uedono, Y. Tsukada, Y. Mikawa, T. Mochizuki, H. Fujisawa, H. Ikeda, K. Kurihara, K. Fujito, S. Terada, S. Ishibashi, and S. F. Chichibu, "Vacancies and electron trapping centers in acidic ammonothermal GaN probed by a monoenergetic positron beam," *J. Cryst. Growth* **448**, 117–121 (2016).
- <sup>60</sup>H. Sakurai, M. Omori, S. Yamada, Y. Furukawa, H. Suzuki, T. Narita, K. Kataoka, M. Horita, M. Bockowski, J. Suda, and T. Kachi, "Highly effective activation of Mg-implanted *p*-type GaN by ultra-high-pressure annealing," *Appl. Phys. Lett.* **115**, 142104 (2019).
- <sup>61</sup>K. Sierakowski, R. Jakiel, B. Lucznik, P. Kwiatkowski, M. Iwinska, M. Turek, H. Sakurai, T. Kachi, and M. Bockowski, "High pressure processing of ion implanted GaN," *Electronics* **9**, 1380 (2020).
- <sup>62</sup>P. C. Clapp, "Atomic configurations in binary alloys," *Phys. Rev. B* **4**, 255–270 (1971).
- <sup>63</sup>C. G. Van de Walle and J. Neugebauer, "First-principles calculations for defects and impurities: Applications to III-nitrides," *J. Appl. Phys.* **95**, 3851–3879 (2004).
- <sup>64</sup>A. Uedono, J. Takino, T. Sumi, Y. Okayama, M. Imanishi, S. Ishibashi, and Y. Mori, "Vacancy-type defects in bulk GaN grown by oxide vapor phase epitaxy probed using positron annihilation," *J. Cryst. Growth* **570**, 126219 (2021).
- <sup>65</sup>F. Tuomisto, V. Norrman, and I. Makkonen, "On the sensitivity of positron annihilation signals to alloy homogeneity in In<sub>x</sub>Ga<sub>1-x</sub>N," *J. Phys.: Conf. Ser.* **505**, 012042 (2014).
- <sup>66</sup>A. Uedono, S. Ishibashi, K. Tenjinbayashi, T. Tsutsui, K. Nakahara, D. Takamizu, and S. F. Chichibu, "Defect characterization in Mg-doped GaN studied using a monoenergetic positron beam," *J. Appl. Phys.* **111**, 014508 (2012).
- <sup>67</sup>C. E. Dreyer, A. Alkauskas, J. L. Lyons, J. S. Speck, and C. G. Van de Walle, "Gallium vacancy complexes as a cause of Shockley-Read-Hall recombination in III-nitride light emitters," *Appl. Phys. Lett.* **108**, 141101 (2016).
- <sup>68</sup>Q. Yan, A. Janotti, M. Scheffler, and C. G. Van de Walle, "Origins of optical absorption and emission lines in AlN," *Appl. Phys. Lett.* **105**, 111104 (2014).
- <sup>69</sup>D. J. Keeble, R. A. Mackie, W. Egger, B. Löwe, P. Pikart, C. Hugenschmidt, and T. J. Jackson, "Identification of vacancy defects in a thin film perovskite oxide," *Phys. Rev. B* **81**, 064102 (2010).
- <sup>70</sup>D. J. Keeble, S. Wicklein, R. Dittmann, L. Ravelli, R. A. Mackie, and W. Egger, "Identification of *a*- and *b*-site cation vacancy defects in perovskite oxide thin films," *Phys. Rev. Lett.* **105**, 226102 (2010).
- <sup>71</sup>M. M. Rutkowski, K. McNicholas, Z. Q. Zeng, F. Tuomisto, and L. J. Brillson, "Optical identification of oxygen vacancy formation at SrTiO<sub>3</sub>–(Ba,Sr)TiO<sub>3</sub> heterostructures," *J. Phys. D: Appl. Phys.* **47**, 255303 (2014).
- <sup>72</sup>N. M. Dawley, B. H. Goodge, W. Egger, M. R. Barone, L. F. Kourkoutis, D. J. Keeble, and D. G. Schlom, "Defect accommodation in off-stoichiometric

- (SrTiO<sub>3</sub>)<sub>n</sub>SrO Ruddlesden-Popper superlattices studied with positron annihilation spectroscopy," *Appl. Phys. Lett.* **117**, 062901 (2020).
- <sup>73</sup>A. Karjalainen, V. Prozheeva, I. Makkonen, C. Guguschev, T. Markurt, M. Bickermann, and F. Tuomisto, "TiSr antisite: An abundant point defect in SrTiO<sub>3</sub>," *J. Appl. Phys.* **127**, 245702 (2020).
- <sup>74</sup>A. Karjalainen, V. Prozheeva, K. Simula, I. Makkonen, V. Callewaert, J. B. Varley, and F. Tuomisto, "Split Ga vacancies and the unusually strong anisotropy of positron annihilation spectra in  $\beta$ -Ga<sub>2</sub>O<sub>3</sub>," *Phys. Rev. B* **102**, 195207 (2020).
- <sup>75</sup>A. Karjalainen, I. Makkonen, J. Etula, K. Goto, H. Murakami, Y. Kumagai, and F. Tuomisto, "Split Ga vacancies in *n*-type and semi-insulating  $\beta$ -Ga<sub>2</sub>O<sub>3</sub> single crystals," *Appl. Phys. Lett.* **118**, 072104 (2021).
- <sup>76</sup>A. Karjalainen, P. M. Weiser, I. Makkonen, V. M. Reinertsen, L. Vines, and F. Tuomisto, "Interplay of vacancies, hydrogen, and electrical compensation in irradiated and annealed *n*-type  $\beta$ -Ga<sub>2</sub>O<sub>3</sub>," *J. Appl. Phys.* **129**, 165702 (2021).
- <sup>77</sup>J. Jesenovec, M. H. Weber, C. Pansegrau, M. D. McCluskey, K. G. Lynn, and J. S. McCloy, "Gallium vacancy formation in oxygen annealed  $\beta$ -Ga<sub>2</sub>O<sub>3</sub>," *J. Appl. Phys.* **129**, 245701 (2021).
- <sup>78</sup>S. K. Swain, M. H. Weber, J. Jesenovec, M. Saleh, K. G. Lynn, and J. S. McCloy, "Compensation of shallow donors by gallium vacancies in monoclinic  $\beta$ -Ga<sub>2</sub>O<sub>3</sub>," *Phys. Rev. Appl.* **15**, 054010 (2021).
- <sup>79</sup>J. B. Varley, H. Peelaers, A. Janotti, and C. G. V. de Walle, "Hydrogenated cation vacancies in semiconducting oxides," *J. Phys.: Condens. Matter* **23**, 334212 (2011).
- <sup>80</sup>Y. K. Frodason, J. B. Varley, K. M. H. Johansen, L. Vines, and C. G. Van de Walle, "Migration of Ga vacancies and interstitials in  $\beta$ -Ga<sub>2</sub>O<sub>3</sub>," *Phys. Rev. B* **107**, 024109 (2023).
- <sup>81</sup>A. Azarov, J. G. Fernández, J. Zhao, F. Djurabekova, H. He, R. He, Ø. Prytz, L. Vines, U. Bektas, P. Chekhonin, N. Klingner, G. Hlawacek, and A. Kuznetsov, "Universal radiation tolerant semiconductor," *Nat. Commun.* **14**, 4855 (2023).
- <sup>82</sup>P. Gordo, L. Liszkay, Z. Kajcsos, K. Havancsák, V. Skuratov, G. Kögel, P. Sperr, W. Egger, A. de Lima, and M. Ferreira Marques, "On the defect pattern evolution in sapphire irradiated by swift ions in a broad fluence range," *Appl. Surf. Sci.* **255**, 254–256 (2008), Proceedings of the Eleventh International Workshop on Slow Positron Beam Techniques for Solids and Surfaces.
- <sup>83</sup>V. Prozheeva, R. Hölldbler, H. von Wenckstern, M. Grundmann, and F. Tuomisto, "Effects of alloy composition and Si-doping on vacancy defect formation in (In<sub>x</sub>Ga<sub>1-x</sub>)<sub>2</sub>O<sub>3</sub> thin films," *J. Appl. Phys.* **123**, 125705 (2018).
- <sup>84</sup>C. J. Edwardson, P. G. Coleman, D. J. Paez, J. K. Doylend, and A. P. Knights, "Direct observation of electron capture and reemission by the divacancy via charge transient positron spectroscopy," *Phys. Rev. Lett.* **110**, 136401 (2013).
- <sup>85</sup>M. Maekawa, H. Abe, A. Miyashita, S. Sakai, S. Yamamoto, and A. Kawasuso, "Vacancy-induced ferromagnetism in ZnO probed by spin-polarized positron annihilation spectroscopy," *Appl. Phys. Lett.* **110**, 172402 (2017).
- <sup>86</sup>M. Maekawa, A. Miyashita, S. Sakai, and A. Kawasuso, "Gadolinium-implanted GaN studied by spin-polarized positron annihilation spectroscopy," *Phys. Rev. B* **102**, 054427 (2020).
- <sup>87</sup>P. Or, T. R. Devidas, T. Taniguchi, K. Watanabe, I. Sabo-Napadesky, S. May-Tal Beck, G. Ron, and H. Steinberg, "Positron charge sensing using a double-gated graphene field effect transistor," *Rev. Sci. Instrum.* **93**, 015002 (2022).
- <sup>88</sup>Y. Nagai, M. Hasegawa, Z. Tang, A. Hempel, K. Yubuta, T. Shimamura, Y. Kawazoe, A. Kawai, and F. Kano, "Positron confinement in ultrafine embedded particles: Quantum-dot-like state in an Fe-Cu alloy," *Phys. Rev. B* **61**, 6574–6578 (2000).
- <sup>89</sup>N. D. Drummond, P. López Ríos, R. J. Needs, and C. J. Pickard, "Quantum monte carlo study of a positron in an electron gas," *Phys. Rev. Lett.* **107**, 207402 (2011).
- <sup>90</sup>Y. Kita, R. Maezono, M. Tachikawa, M. D. Towler, and R. J. Needs, "Ab initio quantum Monte Carlo study of the binding of a positron to alkali-metal hydrides," *J. Chem. Phys.* **135**, 054108 (2011).
- <sup>91</sup>K. A. Simula, J. E. Muff, I. Makkonen, and N. D. Drummond, "Quantum Monte Carlo study of positron lifetimes in solids," *Phys. Rev. Lett.* **129**, 166403 (2022).
- <sup>92</sup>K. A. Simula, J. Häkkinen, I. Zhelezova, N. D. Drummond, F. Tuomisto, and I. Makkonen, "Quantum Monte Carlo study of Doppler broadening of positron annihilation radiation in semiconductors and insulators," *Phys. Rev. B* **108**, 045201 (2023).
- <sup>93</sup>K. A. Simula and I. Makkonen, "Calculation of the energies of the multideterminant states of the nitrogen vacancy center in diamond with quantum Monte Carlo," *Phys. Rev. B* **108**, 094108 (2023).
- <sup>94</sup>J. Hofierka, B. Cunningham, C. M. Rawlins, C. H. Patterson, and D. G. Green, "Many-body theory of positron binding to polyatomic molecules," *Nature* **606**, 688–693 (2022).
- <sup>95</sup>V. Callewaert, R. Saniz, B. Barbiellini, A. Bansil, and B. Partoens, "Application of the weighted-density approximation to the accurate description of electron-positron correlation effects in materials," *Phys. Rev. B* **96**, 085135 (2017).
- <sup>96</sup>W. Shi, V. Callewaert, B. Barbiellini, R. Saniz, M. Butterling, W. Egger, M. Dickmann, C. Hugenschmidt, B. Shakeri, R. W. Meulenbergh, E. Brück, B. Partoens, A. Bansil, and S. W. H. Eijt, "Nature of the positron state in CdSe quantum dots," *Phys. Rev. Lett.* **121**, 057401 (2018).
- <sup>97</sup>K. O. Jensen and A. B. Walker, "Non-local positron-electron density functional theory and the positron surface state," *J. Phys. F: Met. Phys.* **18**, L277 (1988).
- <sup>98</sup>A. Rubaszek, "Electron-positron enhancement factors at a metal surface: Aluminum," *Phys. Rev. B* **44**, 10857–10868 (1991).
- <sup>99</sup>Q. Yang, Z. Hu, I. Makkonen, P. Desgardin, W. Egger, M.-F. Barthé, and P. Olsson, "A combined experimental and theoretical study of small and large vacancy clusters in tungsten," *J. Nucl. Mater.* **571**, 154019 (2022).
- <sup>100</sup>A. Alkauskas, J. L. Lyons, D. Steiauf, and C. G. Van de Walle, "First-principles calculations of luminescence spectrum line shapes for defects in semiconductors: The example of GaN and ZnO," *Phys. Rev. Lett.* **109**, 267401 (2012).
- <sup>101</sup>A. Alkauskas, Q. Yan, and C. G. Van de Walle, "First-principles theory of nonradiative carrier capture via multiphonon emission," *Phys. Rev. B* **90**, 075202 (2014).
- <sup>102</sup>C. E. Dreyer, A. Alkauskas, J. L. Lyons, and C. G. Van de Walle, "Radiative capture rates at deep defects from electronic structure calculations," *Phys. Rev. B* **102**, 085305 (2020).
- <sup>103</sup>F. Zhao, M. E. Turiansky, A. Alkauskas, and C. G. Van de Walle, "Trap-assisted Auger-Meitner recombination from first principles," *Phys. Rev. Lett.* **131**, 056402 (2023).